NATIONAL ENERGY TECHNOLOGY LABORATORY

Natural Gas Hydrates Research Portfolio

Quarterly Progress Report
FY14-Q4

Yongkoo Seol, ORD Technical Coordinator

Delivery Date: November 20, 2014

Prepared by
U.S. Department of Energy
National Energy Technology Laboratory
Office of Research and Development

Prepared for
U.S. Department of Energy
National Energy Technology Laboratory
Strategic Center for Natural Gas and Oil

U.S. DEPARTMENT OF ENERGY

List of Authors

Yongkoo Seol, ORD Technical Coordinator

Gary Sames, ORD Project Coordinator

Cynthia Powell, ORD Focus Area Lead (*Acting*)

Jeffery Ilconich, RES Activity Manager

Table of Contents

List of Figures

List of Tables

Acronym List

Acronym	Descriptive Name
2D	Two-Dimensional
3D	Three-Dimensional
AK-DNR	Alaskan Department of Natural Resources
ANS	Alaska North Slope
Be	Beryllium
CMU	Carnegie Mellon University
CO_2	Carbon Dioxide
CSM	Colorado School of Mines
CT	Computed Tomography
DOE	Department of Energy
DT	Sonic
FAL	Focus Area Lead
FEHM	Finite Element/Finite Volume Heat and Mass Transfer Computer Code
FPM	Federal Project Manager
FWP	Field Work Proposal
GR	Gamma Ray
GUI	Graphical User Interface
HBS	Hydrate-Bearing Sediment
HQ	Headquarters
HRS	HydrateResSim
MST	Multi-Stage Tests
NETL	National Energy Technology Laboratory
NMR	Nuclear Magnetic Resonance
ORD	Office of Research and Development
PBU	Prudhoe Bay Unit
Pitt	University of Pittsburgh
PMP	Project Management Plan
PSU or Penn State	The Pennsylvania State University
R&D	Research and Development
Res	Resistivity
RES	Research and Engineering Services
RHOB	Density
RUA	Regional University Alliance
SARS	Safety Analysis and Review System
SCNGO	Strategic Center for Natural Gas and Oil

Acronym	Descriptive Name
S_H	Hydrate Saturation
SHC	Shale Content
SMP	Spatially Mobilized Plane
SOPO	Statement of Project Objectives
SST	Single-Stage Tests
S_W	Water Saturation
TC	Technical Coordinator
TCD	Thermal Conductivity Detector
THM	Thermal-hydrological-geomechanical
TM	Technology Manager
TMo	Technical Monitor
TVDSS	Total Vertical Depth
URS	URS Corporation
USGS	United States Geological Survey
VSHC	Volume of Shale Content
WVU	West Virginia University

1.0 Annual Executive Summary

The National Methane Hydrate Research and Development (R&D) Program has worked to accelerate the determination and realization of gas hydrate's resource potential and to better understand the role of gas hydrate in the environment. This Natural Gas Hydrates Research project was developed with a diverse set of research activities, performed by the U.S. Department of Energy (DOE), National Energy Technology Laboratory (NETL), Office of Research and Development (ORD), to fill multiple needs within the National Gas Hydrate R&D program.

Continuing efforts on numerical simulations include history matching for the Iġnik Sikumi field test for the gas hydrate exchange trial using Mix3HydrateResSim (Subtask 2.1). A series of reservoir simulations were performed to model the long-term response to depressurization (Subtask 2.2). Laboratory experiments continued, particularly in the area of geomechanical tests on mechanical strength measurements with hydrate-bearing sediments (Subtask 3.1). A spatially mobilized plane (SMP) subloading critical state constitutive model was developed and verified upon the available data from the laboratory test, as well as literature using modified geomechanics code (Subtask 3.2). CO_2-CH_4 gas exchange kinetics and mechanisms tests (Task 4.0) were also performed through batch and column tests utilizing high resolution Raman spectrometer. The X-ray transparent, high pressure Beryllium vessel and the NETL X-ray micro-computed tomography (CT) have been deployed for imaging hydrate pore habits in sands to execute pore scale characterization of hydrate-bearing sediments (Subtask 5.1). A pore network modeling method was used to investigate the effects of hydrate pore habit and morphology on flow properties, including hydraulic conductivity, tortuosity, and relative permeability based on two-dimensional (2D) and three-dimensional (3D) pore networks extracted from X-ray CT images (Subtask 5.2).

This annual report provides the list of tasks, status of the work, major accomplishments, and updates regarding milestone dates. Research highlights this quarter include:

- Geostatistical representations of the Prudhoe Bay Unit (PBU)-based system incorporating extensive well-log correlations and a 3D representation of the fault-bounded Mount Elbert system have been generated to more extensive and computationally expensive simulation results.
- A series of code comparison problems including a CO_2 injection scenario in a 2D reservoir system filled with CH_4 hydrate was developed for distribution to the code comparison group.
- A multi-property characterization chamber for geophysical-hydrological investigations of hydrate bearing sediments was developed. The unique device allows researchers to characterize hydrate bearing sediments for geomechanical, acoustic, and hydrological properties. A peer-reviewed article was published in *Review of Scientific Instruments*. A method to compensate the effect of the thick rubber sleeve was developed along with a set of controlled tests with rubber rods. This method was applied when calculating the deviator stress on CH_4-hydrate-bearing sediment (HBS) samples. The modification of the acoustic sensor unit with the addition of a backing layer improved the S-wave identification from ringing noises in piezocrystal.
- An inter-laboratory study with Colorado School of Mines (CSM) and the U.S. Geological Survey (USGS) was conducted on the non-cementing hydrate formation method developed by NETL. Both partner laboratories were provided with a series of acoustic data, monitored during the non-cementing hydrate formation.

- Comparison between the single-stage tests (SST) and the multi-stage tests (MST) confirm that with the MST, the stiffness of HBS subjected to the subsequent stage of confining pressure can be greater than that with the SST under similar confining pressure, due to the axial overloading at the precedent stage. In contrast, the strength of HBS can barely be affected by the previous loading history, as presented in the previous report. Our test results of geomechanical properties of non-cementing CH_4-HBS samples were compared with those of other research groups. Compressive strength (maximum deviator stress) data appeared to be in good agreement.
- A constitutive model was developed for sediments containing methane hydrates. Using geomechanics software coupling a geomechanics code, FLAC3D, with a multiphase flow code, TOUGH+, analysis was performed to test and validate the developed constitutive model.
- A laboratory-scale production test, using CO_2-CH_4 gas exchange technique, was performed for extended hours. The cumulative recovery of the CH_4 from CO_2 and N_2, injected with CH_4-hydrate bearing sediments with the presence of free water, reached up to 35 percent, which is significantly larger than the estimation from previous batch tests, but lower than expected based on literature value (up to 80 percent). The presence of free water in the pore space would be associated with the lower than expected CH_4 recovery rates.
- A high resolution Raman spectrometer was set-up for examining the gas exchange mechanism, providing detailed spectra for various molecular bondings. However, the current data set does not provide evidence for change in the hydrate lattice during the gas exchange process and free water released during the exchange.
- The X-ray transparent, high pressure Beryllium (Be) vessel and the NETL X-ray micro-CT have been deployed for imaging hydrate pore habits in sands. A delay in the gas line inspection in the CT lab has not allowed for CT images of hydrate-bearing sediments to be obtained. Instead, fundamentals of X-ray characterization of analogue specimens were explored, in which the hydrate phase is replaced by polyurethane spheroids with density identical to that of hydrate. In addition, CT image reconstruction techniques have been investigated for better (water and hydrate) phase separation. The team was able to form methane hydrate within the Be vessel and collect X-ray CT images of hydrate-bearing sediments in the laboratory. This has provided a solid base for the FY15 research project.
- A pore network modeling method was used to investigate the effects of hydrate pore habit and morphology on flow properties, including hydraulic conductivity, tortuosity, and relative permeability. A set of 2D pore networks have been used for parameter studies. 3D pore networks extracted from X-ray CT images of dried soil specimens, including soils from the Mallik hydrate site, have been used for relative permeability computations.

2.0 Milestones

The status of the M-1 milestones is presented below.

Major Goals of the Project – Hydrates_2013.07.02

Milestone Identifier	Milestone Title	Planned Completion Date	Actual/ Forecast Completion	Method of Verification	Comments
Task 2.0 Reservoir Simulation of Gas Hydrates Production Field Tests					
M1.14.2.A	Development and distribution of elementary problem sets for code comparison study.	12/31/2013	04/30/2014	Public release of elementary problem sets (Subtask 2.1, 12/13).	Completed.
M1.14.2.B	Development and distribution of Iğnik Sikumi-based problem sets for code comparison study.	04/30/2014	04/30/2014	An Iğnik Sikumi-based problem (Subtask 2.1, 04/14).	Completed.
M1.14.2.C	Complete simulations of production and flow modeling representative of a long-term depressurization test and modeling-based assessment of the potential for methane production from CO_2/N_2 exchange test.	06/30/2014	09/30/2014	One or more ICGH 8 manuscripts on the results of the production scenario simulations (Subtask 2.2, 07/14).	Completed. Site selection and new dataset delayed the progress.
Task 3.0 Developing Constitutive Models of Various Hydrate-Bearing Sands					
M1.14.3.A	Complete tri-axial geomechanical strength and deformability tests on CH_4 and CO_2-hydrate-bearing sediments.	03/31/2014	09/30/2014	A report summarizing the experimental work completed (Subtask 3.1, 03/14).	Completed. CO_2 hydrate mechanical test.
M1.14.3.B	Complete data analysis for tri-axial tests and development of a constitutive model defining the relationship between hydrate saturation and elastoplastic soil behavior parameters.	09/30/2014	11/14/2014	Manuscripts on the testing program and constitutive modeling (Subtask 3.2, 09/14).	Delayed.

Milestone Identifier	Milestone Title	Planned Completion Date	Actual/ Forecast Completion	Method of Verification	Comments
Task 4.0 Assessment of Gas Exchange Processes of CH_4 Hydrate with CO_2 under Reservoir Conditions					
M1.14.4.A	Complete CO_2 (and/or CO_2/N_2 mixture) - CH_4 gas exchange mechanism tests with Raman spectroscopy.	03/31/2014	09/30/2014	Manuscript on gas exchange mechanism investigated with Raman spectroscopy (Subtask 4.1).	Completed. No evidence was identified for free water release.
M1.14.4.B	Complete the measurements of CO_2 (and/or CO_2/N_2 mixture) - CH_4 exchange kinetics with the presence of free water.	03/31/2014	06/30/2014		Completed.
M1.14.4.C	Complete comparative analysis for gas exchange kinetics data from experiments conducted at: NETL, LBNL, and PNNL (if available).	06/30/2014	06/30/2014	Manuscript on gas exchange kinetics of various hydrate-bearing sediments (Subtasks 4.2-3).	Completed. No data available from LBNL or PNNL.
Task 5.0 Pore Scale Visualization and Characterization of Hydrate-Bearing Sediments					
M1.14.5.A	Complete development of pore scale imaging procedures and collection of hydrate images of hydrate-bearing sediments.	03/31/2014	03/31/2014	Public release of high resolution images of pore spaces showing hydrate accumulation patterns.	Completed.
M1.14.5.B	Complete development of grain scale constitutive models for hydrate-bearing sediments based on CT images.	09/30/2014	09/30/2014	Manuscript on pore scale visualization of hydrate-bearing sediments and grain-scale constitutive models.	Completed.

Major Goals of the Project – Hydrates_FY15

Milestone Identifier	Milestone Title	Planned Completion Date	Actual/ Forecast Completion	Method of Verification	Comments
Task 2.0 Reservoir Simulation of Gas Hydrates Production Field Tests					
M1.15.2.A	Analysis of Iġnik Sikumi #1 code comparison problem for code comparison and analysis.	12/31/2014		Series of manuscripts on the Iġnik Sikumi history match from the Code Comparison Group (Subtask 2.2).	
M1.15.2.B	Complete simulations of production and flow modeling from a long-term depressurization test at the site chosen for the field test.	06/30/2015		Manuscript on depressurization test scenarios on the Alaska North Slope (Subtask 2.1).	
M1.15.2.C	Analysis of a Marine hydrate-based problem for code comparison and analysis.	09/30/2015			
Task 3.0 Laboratory Hydrologic and Geomechanical Characterization and Analysis of Hydrate-Bearing Sediments					
M1.15.3.A	Demonstration of core flow equipment and personnel capability to conduct the relative permeability test on hydrate-bearing sediments.	12/31/2014		Improved mobile gas hydrate testing unit with additional gas/fluid mass flow meters and temperature chamber (Subtask 3.1).	
M1.15.3.B	Complete relative permeability tests on various types of sediment textures at different hydrate saturations and effective confining stresses and porosities.	03/30/2015		Report on relative permeability of HBS (Subtask 3.1).	
M1.15.3.C	Complete a working TOUGH+FLAC framework.	03/30/2015	06/30/2015	A working TOUGH+FLAC code incorporated constitutive laws for hydrate-bearing soils (Subtask 3.3).	Staff has not been identified.

Milestone Identifier	Milestone Title	Planned Completion Date	Actual/ Forecast Completion	Method of Verification	Comments
M1.15.3.D	Complete tri-axial geomechanical strength and deformability tests on dissociated HBS at various dissociation levels.	06/30/2015		Manuscript on geomechanical strength tests on hydrate-bearing sediment under dissociation condition (Subtask 3.2).	
M1.15.3.E	Complete data analysis for tri-axial tests and development of a constitutive model.	09/30/2015		Manuscripts on the geomechanical tests for HBS under hydrate dissociation condition and constitutive modeling (Subtask 3.3).	
Task 4.0 Pore-Scale Visualization and Characterization of Hydrate-Bearing Sediments					
M1.15.4.A	Complete visualization of hydrate evolutions during brine injection and validate the NETL proposed non-cementing hydrate formation method.	03/31/2015		Report on hydrate evolutions during continuous saline flow and images/videos on this dynamic process (Subtask 4.1).	
M1.15.4.B	Complete design, modification, and manufacture of end pieces for current high-pressure X-ray microCT vessel to have geomechanical measurement capabilities.	06/30/2015		Manuscript on understanding permeability in sediments under heterogeneous pressure distribution during hydrate dissociation (Subtask 4.2).	

Milestone Identifier	Milestone Title	Planned Completion Date	Actual/ Forecast Completion	Method of Verification	Comments
M1.15.4.C	Complete X-ray micro CT imaging for water and gas distributions after hydrate dissociation and implication of flow permeability during dissociation.	09/30/2015		Report on process monitoring using wave velocity and CT scanning in hydrate-bearing sediments, focusing on effects of hydrate morphology, particularly for common hydrate morphologies in nature such as patchy and veins (Subtask 4.3).	
M1.15.4.D	Development of a microfluidic, 2D system for flow and permeability determination.	09/30/2015		Report on the 2D Microfluidic flow tests (Subtask 4.4).	

Note: The Hydrates FY15 FWP was written at the originally requested $800K scope, funded by FY14 (~$469K) and FY15 (~$330K) funds. However, due to the unpredictable circumstances regarding site-support contracts for university faculties and students, all activities within the Statement of Project Objectives will not be initiated until qualified researchers or students are identified. The activities that will not be initiated until full staff supporting is identified are highlighted in gray.

3.0 FY Budgetary Information

The cost performance histograms below show the planned and actual costs and variance for the current budget year.

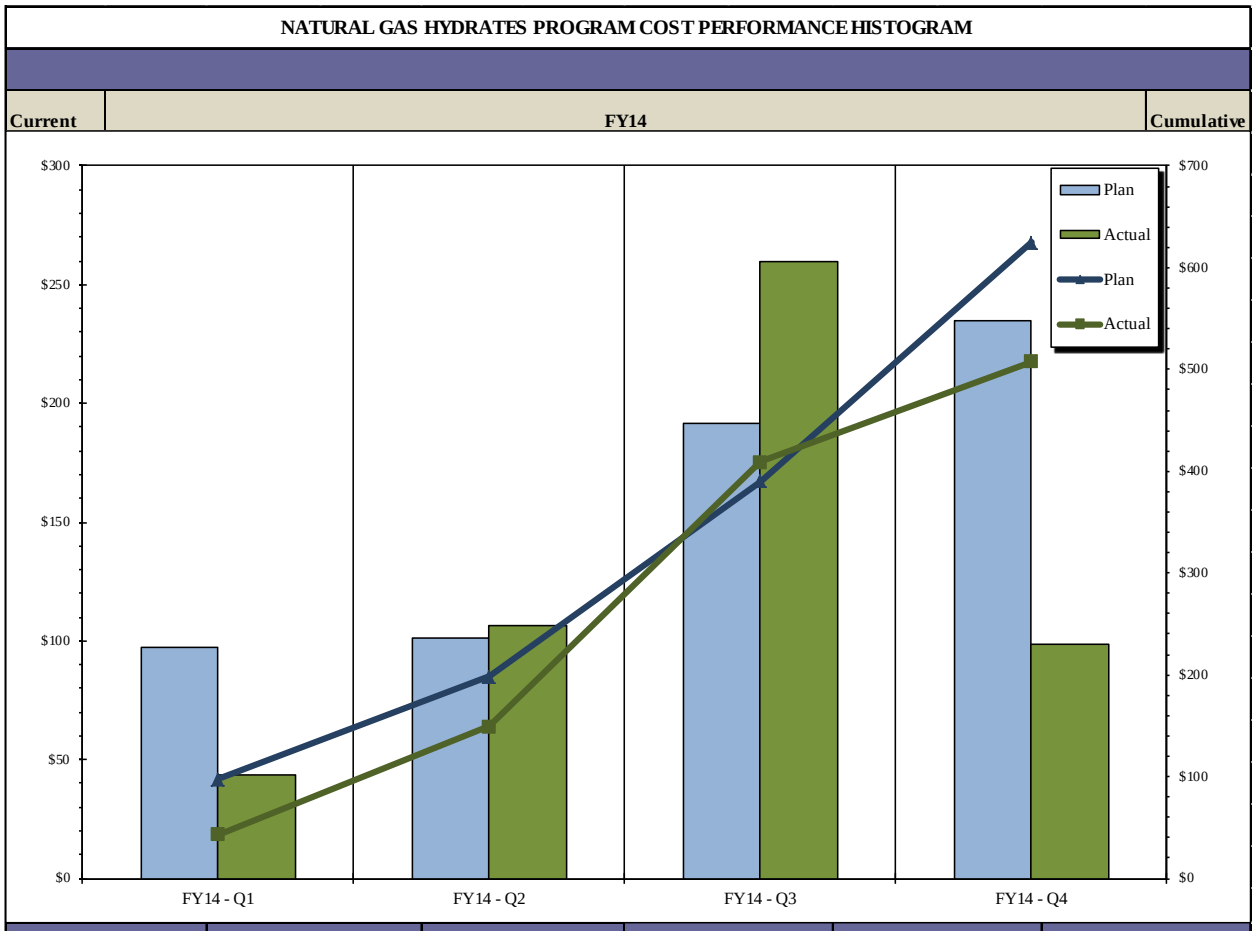

	FY14 - Q1	FY14 - Q2	FY14 - Q3	FY14 - Q4	TOTAL
Current Period					
Plan	$98	$101	$192	$235	$625
Actual	$43	$106	$260	$99	$508
Cumulative					
Plan	$98	$199	$390	$625	$625
Actual	$43	$150	$409	$508	$508

Natural Gas Hydrates Research Portfolio Cost Performance Histogram ($ x 1,000) (Hydrates_2013.07.02)

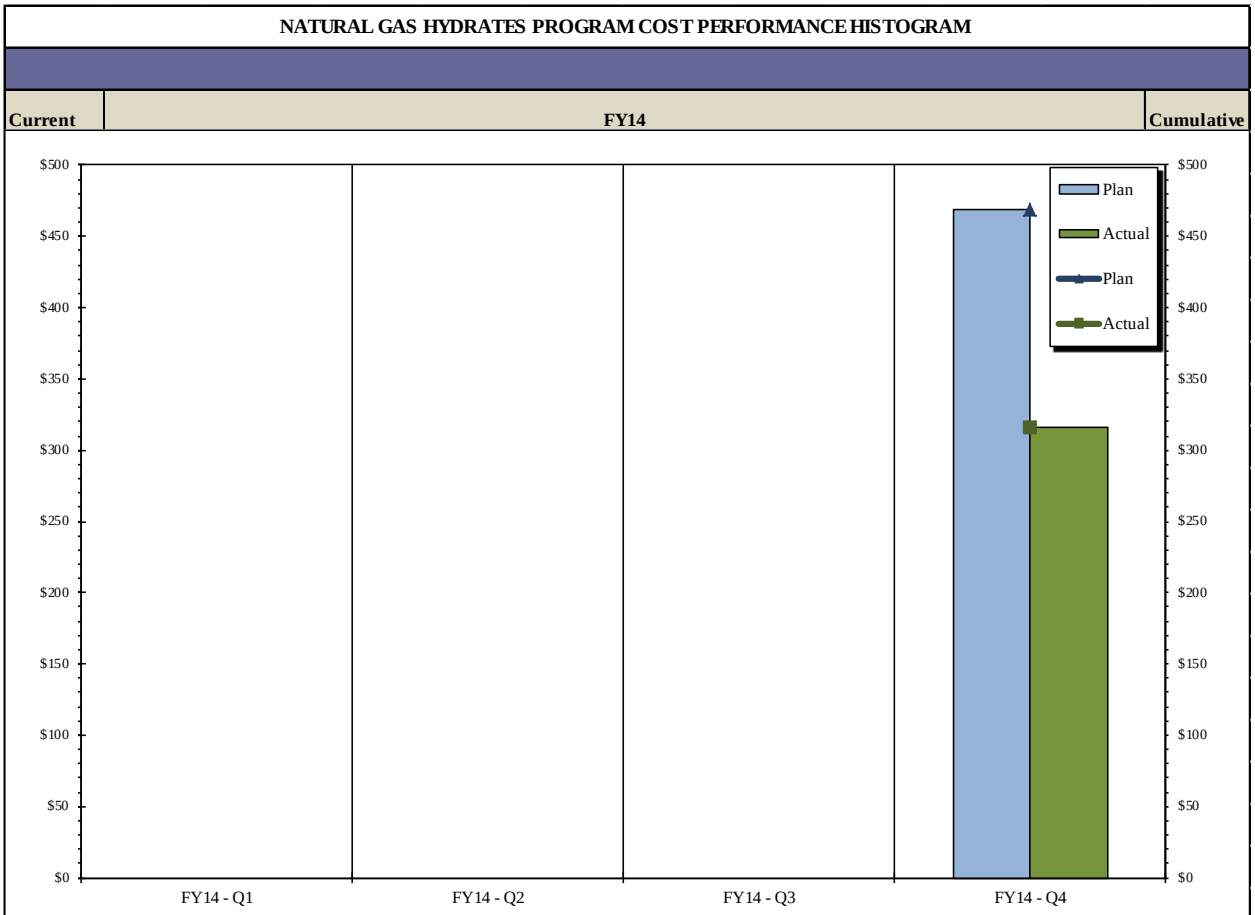

	FY14 - Q1	FY14 - Q2	FY14 - Q3	FY14 - Q4	TOTAL
Current Period					
Plan				$469	$469
Actual				$316	$316
Cumulative					
Plan				$469	$469
Actual				$316	$316

Natural Gas Hydrates Research Portfolio Cost Performance Histogram ($ x 1,000) (Hydrates_FY15)

Variance Explanation:

The budget (plan) for FY14-Q4 was $469K while the actual cost was $316K, resulting in a cost variance of $153K. Cumulative to date, the budget (plan) was $469K while the actual cost was $316K, resulting in a cost variance of $153K. The FY14 variance will be spent in support of the Hydrates FY15 effort.

4.0 Technical Progress

Fiscal Year 2014 Quarter 4

Accomplishments

Hydrates_2013.07.02

Task 1.0 – Project Management and Outreach

The Hydrates FY14-Q3 Quarterly Progress Report was delivered to SCNGO on July 30, 2014.

Task 2.0 Reservoir Simulation of Gas Hydrates Production Field Tests

Subtask 2.1 Simulations of Long-Term Production Scenarios: Depressurization and CO_2 Exchange

In FY14-Q2, simulation results were reported using homogeneous model descriptions for the PBU L-Pad deposits and for a radial representation of the Mount Elbert-like model. This quarter, producing geostatistical representations of the PBU-based system that incorporate extensive well-log correlations and a 3D representation of the fault-bounded Mount Elbert system were the focus. These simulations are much more extensive and computationally expensive than the previous quarter's results.

Subtask 2.2 International Code Comparison Problem Set Based on Iġnik Sikumi

A series of code comparison problems were developed and simulated. Additionally, a CO_2 injection scenario in a 2D reservoir system filled with CH_4 hydrate for distribution to the code comparison group was developed and simulated.

Task 3.0 Developing Constitutive Models of Various Hydrate-Bearing Sands

Subtask 3.1 Laboratory Measurements of Geomechanical Strength and Deformability

The geomechanical test on CO_2-HBS was conducted and completed during this quarter. The non-cementing CO_2-hydrate was formed in three F110 sand + 5% clay samples, and each sample was tested at a single σ'_o. Table 1 shows the general information of samples and conditions utilized in the test. The results of peak deviator stress (q_{peak}) and secant elastic modulus (E_{50}) from the CO_2-HBS were then analyzed in comparison with those from CH_4- and THF-HBS samples.

Table 1: Sample index properties and test conditions of single-stage triaxial drained compression test on CO_2-HBS

Index Properties	Sample #9	Sample #10	Sample #11
Dry Bulk Density, ρ_{dry} (g/ml)	1.66	1.64	1.65
Porosity, ϕ (%)	37.4	38.1	37.5
Hydrate Saturation*, S_h (%)	33.5	37.4	~ 35.0
Hydrate habit	Non-cementing	Non-cementing	Non-cementing
Eff. Confining Pressure, σ'_o (MPa)	2.76	1.38	0.69

* Based on the applied P-T condition, a hydration number of 6.6 was used to calculate the Sh of the current CO_2-HBS samples, while that of 6.2 was used for the Sh calculation of the previous CH_4-HBS samples.

Figure 1 shows that the q_{peak} of non-cementing CO_2-HBS obtained at S_h = ~34–37% is comparable with that of hydrate-free sediment (HFS) sample, which is also observed with CH_4-HBS at the similar S_h. Figure 2, which includes the q_{peak} data of non-cementing CH_4-HBS collected by other research groups, shows noticeable increases in q_{peak} are generally observed when S_h becomes higher than ~40%, at which the hydrate formation habit changes from pore-filling to load-bearing. Upon the extent of the experimental observations from this study and the similar study by [Hyodo et al., 2014], it can be presumed that the q_{peak} (or strength) of CO_2-HBS is comparable to that of CH_4-HBS as long as the index properties of HBS are similar.

The stiffness data of our CO_2-HBS, i.e., the secant elastic moduli, E_{50} (= $q_{50}/\varepsilon_{a,50}$, where q_{50} = 50% of q_{peak} and $\varepsilon_{a,50}$ = axial strain at q_{50}), are compared with those by Yun et al., (2007) over σ'_o in log-log scale (Figure 3). Note that the Yun results were obtained with tetrahydrofuran (THF)-HBS. It is generally known that the elastic modulus (E) is proportional to a power function of σ'_o, i.e., $E \propto \alpha(\sigma'_o)^{\beta}$, where α and β = empirical parameters, and thereby the relationship between the E and σ'_o can be linear in the log-log scale. Both our data and Yun's data show good linear relationships in the log-log scale, and more importantly, despite the difference in the type of guest molecule in hydrate, our data appear to fit well into Yun's data with consideration of S_h. This comparableness indicates that the type of guest molecule may not have a significant effect on the stiffness of HBS, which may also be true for the strength of HBS.

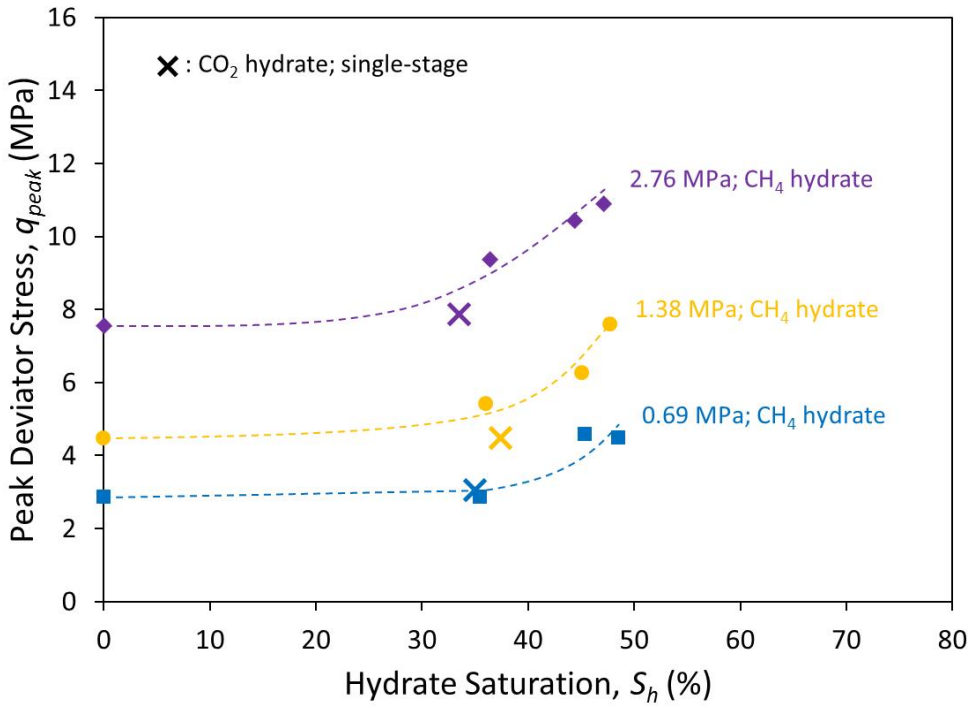

Figure 1: Comparison of q_{peak} between CO_2- and CH_4-HBS samples over various S_h (Note: All data are obtained by NETL).

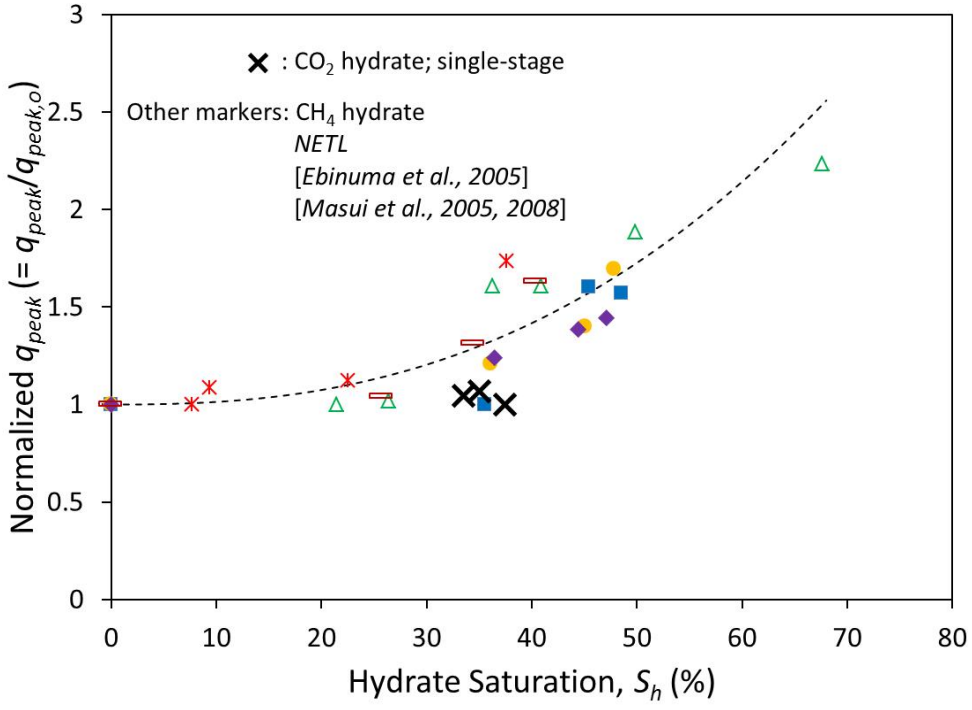

Figure 2: Normalized q_{peak} of CO_2-HBS in comparison with those of CH_4-HBS over various S_h (CH_4-HBS data are collected from [NETL; Ebinuma et al., 2005; Masui et al, 2005, 2008]; q_{peak} is normalized by that of host soil sample, $q_{peak,o}$, i.e., q_{peak} at S_h = 0%, at similar σ'_o).

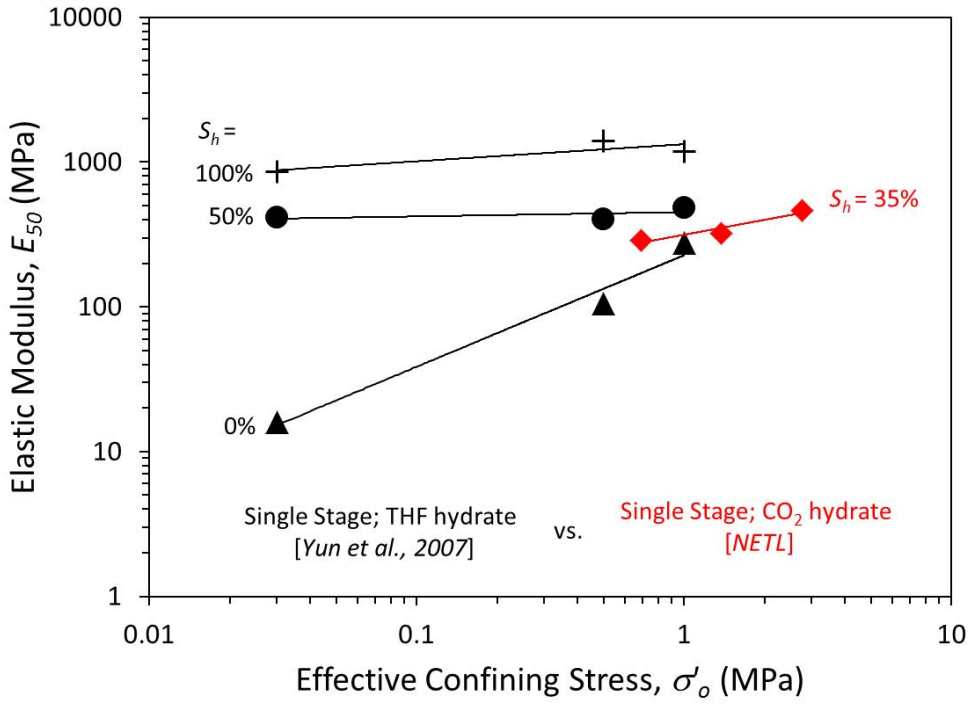

Figure 3: Comparison of E_{50} data obtained from CO_2- and THF-HBS.

Figure 4 shows the stress-strain curves obtained from our CO_2-HBS and hydrate-free sediment (HFS) samples in comparison. Note that the current CO_2-HBS test was conducted with the single-stage test (SST) method, while our previous CH_4-HBS and HFS tests with the multi-stage test (MST) method. It appears in Figure 4 that the q_{peak} of CH_4-HBS (S_h < 40%) is similar to that of HFS (S_h = 0%) at each σ'_o. On the other hand, the initial stiffness (or elastic modulus) of the HFS, particularly at the subsequent σ'_o stage, is obviously greater than the corresponding initial stiffness of the CO_2-HBS. The observation presents obvious influence of axial overloading applied at the precedent σ'_o stage on the stiffness of the HFS, but not on the strength (q_{peak}). The influence of loading history on the stiffness of sediments, which is inherent with the MST method, is readily reconfirmed by calculating the secant elastic moduli, E_{50} (= $q_{50}/\varepsilon_{a,50}$, where q_{50} = 50% of q_{peak} and $\varepsilon_{a,50}$ = axial strain at q_{50}). Figure 5 shows the comparison of our E_{50} results obtained from MST and SST. From the figure, it is clear that when compared relative to the applied σ'_o, the E_{50} data from MST, the non-linearity is shown (i.e., drastic increase in E_{50} at the second and third σ'_o stages) while those from SST shows the linearity.

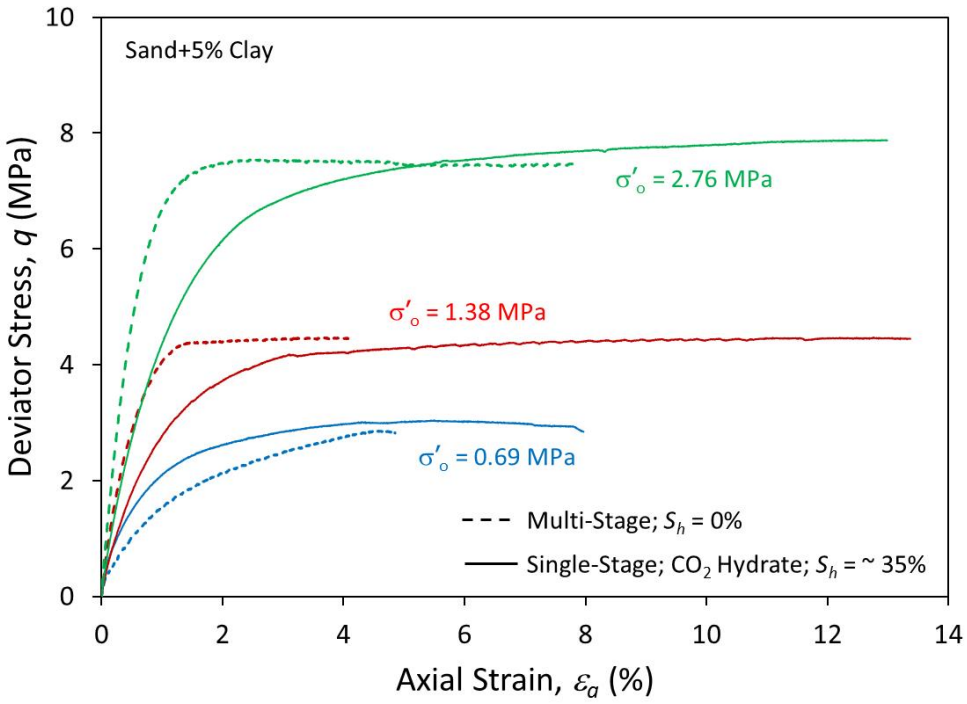

Figure 4: Comparison of stress-strain relationships obtained from multi-stage test (MST) and single-stage test (SST) methods by NETL.

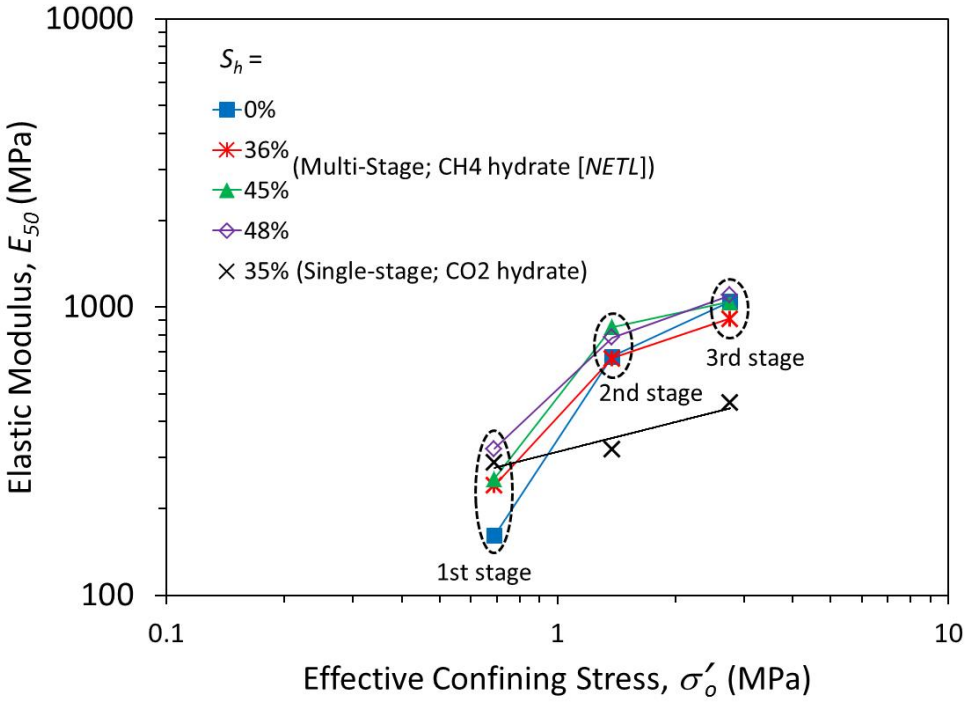

Figure 5: Comparison of elastic moduli (E_{50}), obtained from MST and SST by NETL, over various S_h.

References:

Ebinuma, T., Kamata, Y., Minagawa, H., Ohmura, R., Nagao, J., and Narita, H., "Mechanical Properties of Sandy Sediment Containing Methane Hydrate," proceedings of the 5th International Conference on Gas Hydrates (ICGH 2005), Trondheim, Norway, June 12 – 16, 2005.

Hyodo, M., Li, Y., Yoneda, J., Nakata, Y., Yoshimoto, N., Kajiyama, S., Nishimura, A., and Song, Y., "A Comparative Analysis of the Mechanical Behavior of Carbon Dioxide and Methane Hydrate-Bearing Sediments," *American Mineralogist*, Vol. 99, No. 1, 178–183, 2014.

Masui, A., Haneda, H., Ogata, Y., and Aoki, K., "Effects of Methane Hydrate Formation on Shear Strength of Synthetic Methane Hydrate Sediments," proceedings of the 15th International Offshore and Polar Engineering Conference, Seoul, Korea, June 19 – 24, 2005.

Masui, A., Miyazaki, K., Haneda, H., Ogata, Y., and Aoki, K., "Mechanical Characteristics of Natural and Artificial Gas Hydrate Bearing Sediments," proceedings of the 6th International Conference on Gas Hydrates, Vancouver, British Columbia, Canada, July 6 – 10, 2008.

Yun., T.S., Santamarina, J.C., and Ruppel, C., "Mechanical Properties of Sand, Silt, and Clay Containing Tetrahydrofuran Hydrate," *Journal of Geophysical Research: B-Solid Earth*, Vol. 112, B04106, doi:10.1029/2006 JB 004484, 2007.

Subtask 3.2 Developing Constitutive Models of Various Hydrate-Bearing Sands

Constitutive modeling was performed for coupled geomechanical analysis. The coupled analysis was conducted by coupling the geomechanics code FLAC3D with the multiphase flow code TOUGH+. The coupling framework follows that proposed by Rutqvist and Moridis (2009). From Tough+, the temperature (T), pore pressure (p), and hydrate saturation (S) are updated at each time step. These values are passed to FLAC3D for geomechanical analysis. From FLAC3D, the thermal mechanical analysis is conducted and the resulting changes in the void ratio, permeability are fed back to TOUGH+. The computation then repeats until the end time of an analysis is reached.

For the coupled analysis, a test case was set up in which a methane hydrate bearing sands has the following properties:

Parameters	Hydrate-bearing sands
λ	0.16
κ	0.004
β	2
M	1.1
ν	0.2
t'_{Ncs} (MPa)	23.7
u	7.2
a (MPa)	235
b	1.86
χ_1	1
χ_2	1
h	1
m_o	3
S_H	0.3

Computed drained triaxial compression test results for this material under the confining pressures of 0.3 and 1.0 MPa, respectively, are given in Figures 6 and 7.

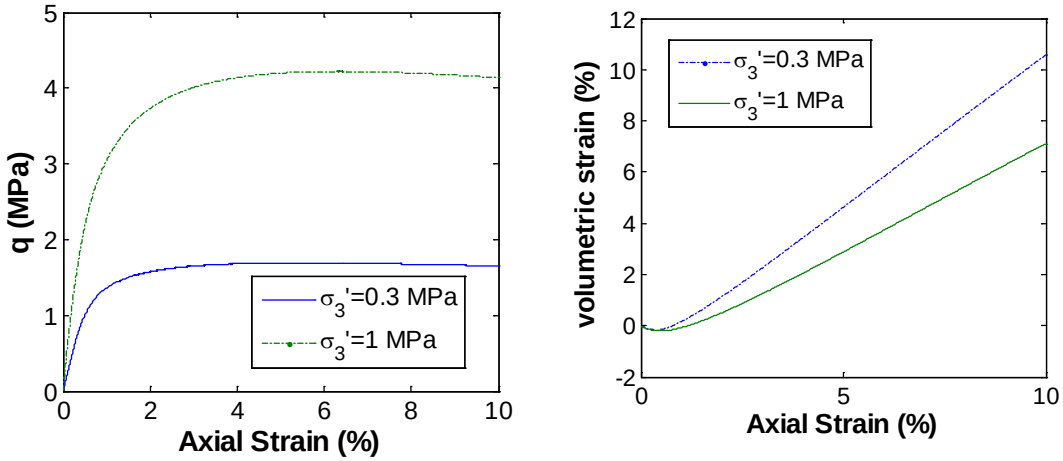

(a) Deviatoric stress versus axial strain (b) Volumetric strain versus axial strain

Figure 6: Stress-strains from drained computed triaxial tests.

If the hydrate is dissociated suddenly at 5% axial strain from SH=30% to zero, the strength of the sand drops substantially as illustrated in Figure 8.

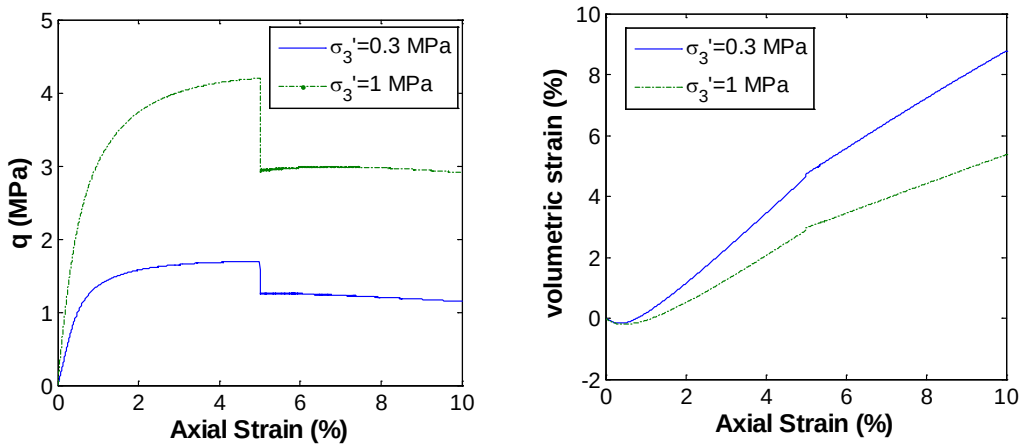

(a) Deviatoric stress versus axial strain (b) Volumetric strain versus axial strain

Figure 7: Stress-strains from drained computed triaxial tests with hydrate dissociation.

For the coupled geomechanical analysis, temperature and pressure were selected such that when the hydrate was dissociated, the aqueous phase contained no ice. The methane dissociation was induced by pumping, and thus pressure was dropped. For the present purpose, the following setup was employed, in which the confining pressure on the sand was 10 MPa; the sand was saturated and under equilibrium with the pore pressure of 9.7 MPa. In other words, the initial effective stress was 0.3 MPa. At the boundary the temperature was kept at 12.5°C, and the pore pressure was kept at 5 MPa. Pumping was carried out at a rate of 0.01 kg/s.

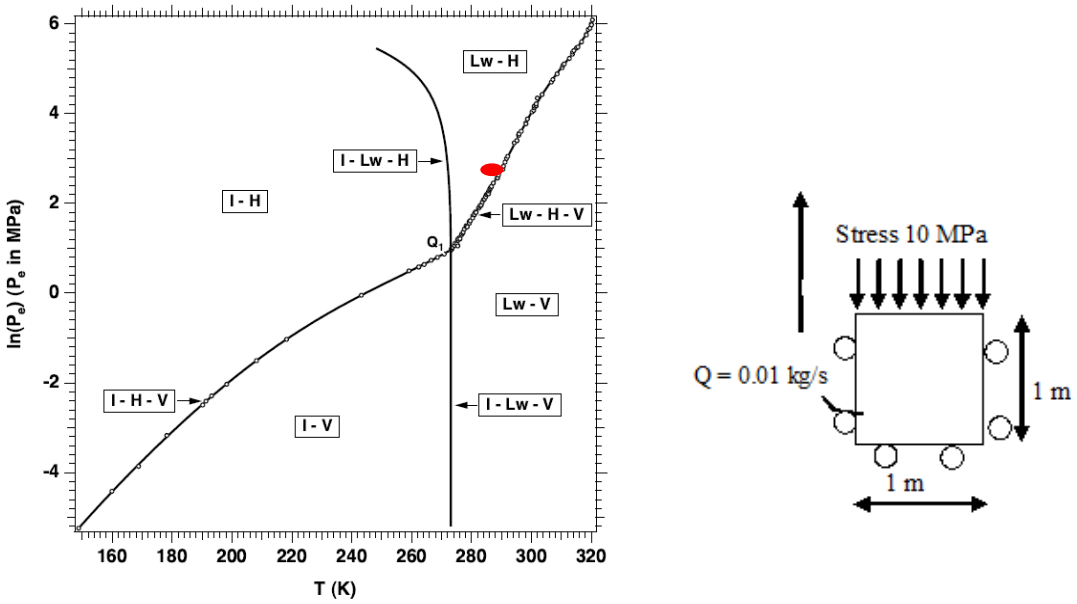

Figure 8: Modeling scenario and initial conditions.

Because of the pumping action and lower pressure at the boundary, both the pore pressure and the temperature in sands changed with time. As a result, hydrate dissociation took place with time, but occurred rather rapidly as shown in Figures 9 and 10. Notice that after the pore pressure dropped to a steady 5 MPa as controlled by the boundary, the temperature stayed at about 6.5°C, and then rose again because the environment had a higher temperature. During the temperature rise, the remaining hydrate completely dissociated. This resulted in the rise of the shear stress and effective confining pressure. The ground settled rapidly initially, and then stabilized when both the pore pressure and temperature reached steady values. The settlement continued, however, once the temperature rose again.

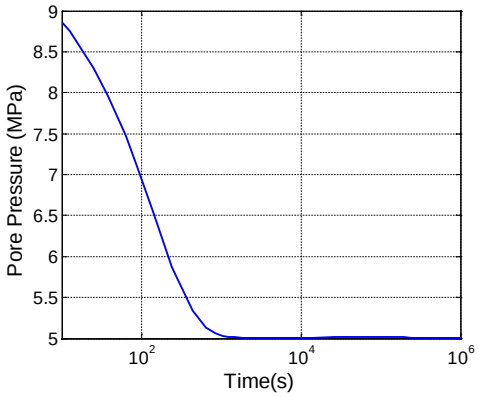

(a) Pore pressure versus time

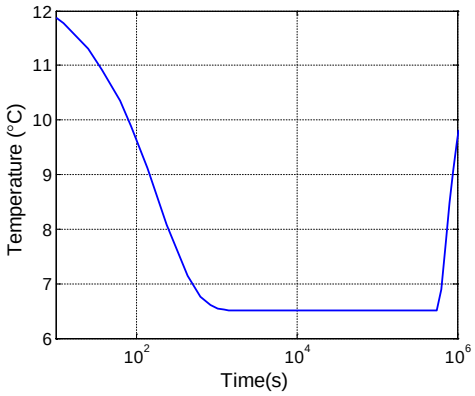

(b) Temperature versus time

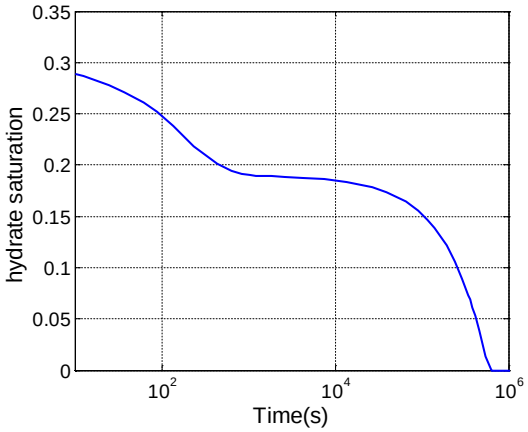

(c) Hydrate saturation versus time

Figure 9: Pumping induced pressure and temperature changes and the dissociation of methane hydrates.

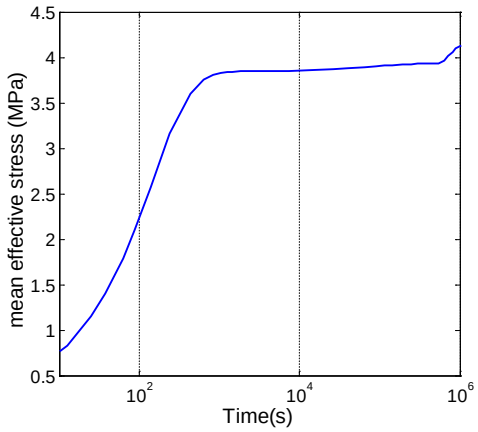

(a) Increase in mean confining stresses

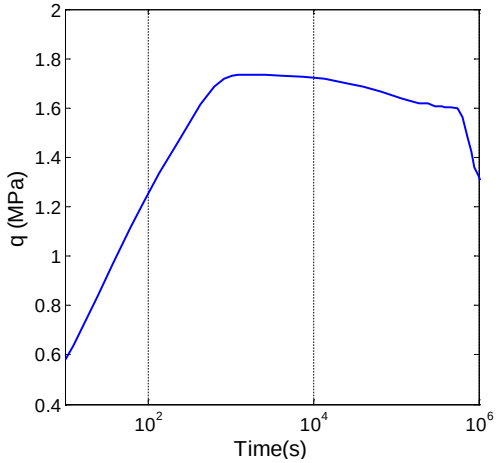

(b) The increase in shear stresses

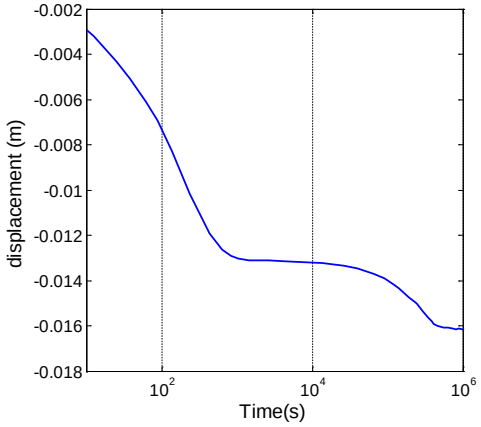

(c) Accumulation of ground settlement

Figure 10: The geomechanical behavior associated with the pumping and hydrate dissociation.

The present analysis demonstrates a successful integration of the developed SMP critical state constitutive model of soils containing methane hydrate with the multiphase flow code. This provides a basis for future exploration of various scenarios in terms of stability of the hydrate bearing deposits under various types of environmental changes including those caused by the efforts to extract methane gas, and global warming.

Reference:

Rutqvist, J., and Moridis, G.J., "Numerical Studies on the Geomechanical Stability of Hydrate-Bearing Sediments," *SPE journal* (Society of Petroleum Engineers (U.S.): 1996), 14:267-82, 2009.

Task 4.0 Assessment of Gas Exchange Processes of CH_4 Hydrate with CO_2 under Reservoir Conditions

Subtask 4.1 Gas Exchange Mechanism with Raman Spectroscopy

Laboratory analysis with Raman spectroscopy was completed to confirm the release of free mobile water from CH_4 hydrate phase. The mobile water release would be an indicator of gas exchange mechanisms through dissociation and reformation of hydrate.

- Hydrate was formed from finely ground ice (5 or 50 wt% D_2O) by pressurizing the vessel with pre-cooled methane gas up to 7.4 MPa at -2°C at isochoric condition. [CO_2 + N_2] mixed gas is charged at a constant flow of 1 ml/min for 5 volumes of head space. The Raman Spectrometer system used was a Laser Quantum IGNIS laser emitting >500mW at 660nm with a Semrock FF667-Di01 dichroic beamsplitter. The Spectrometer was fitted with a grating set to yield a spectral range of -830 cm^{-1} to 5200 cm^{-1} on the ccd array about the laser excitation of 660 nm.
- Gas molecules show their molecular vibration in higher wavelength when they are in gas phase, whereas gas molecules in clathrate cages have the vibrational bands with lower wavelength (Rutqvist and Moridis, 2009). Thus, the gas exchange occurring between [CO_2 + N_2] and CH_4 in the hydrate phase was confirmed through the spectroscopic identification. Figure 11 shows the variation of molecular bands during the gas exchange process. For the 5 wt% D_2O case, peaks representing CO_2 appeared at 1290 and 1384 cm^{-1} and shifted to lower wavelengths of 1280 and 1377 cm^{-1}. Similarly, the peaks of N_2 shifted from 2325 to 2319 cm^{-1}. Simultaneously, the CH_4 band was shifted to a lower wavelength as CH_4 was replaced with [CO_2 + N_2], and the intensity at 2905 cm_{-1} became smaller. These variations in the spectra demonstrate that CO_2 and N_2 spontaneously exchange the CH_4 captured in the hydrate phase.
- The OH and OD bands could be influenced by the hydrogen bonding state of hydrate lattice. Thus, partial dissociation and partial melt make the water band shift or change in intensity. The disappearance of peak at 3067 cm^{-1} was observed in the early stage of gas exchange (Figure 12). To verify whether or not the motion of water molecules is involved in this band, 50 wt% D_2O was used for synthesizing CH_4 hydrate. The band at 3067 cm^{-1} was not found in the 50 wt% D_2O case in CH_4 hydrate and there were no changes in the OD or OH band regions during the exchange process. The current data set is not sufficient to identify the change of hydrate lattice and does not provide evidence for a hydrate exchange mechanism.

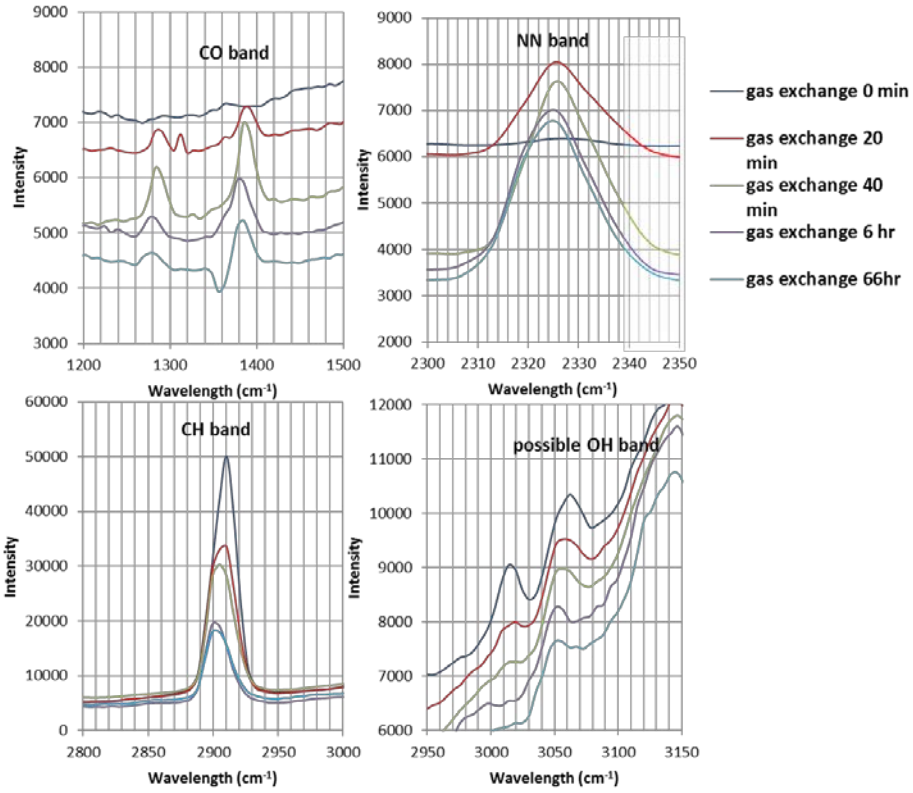

Figure 11: Variation of Raman spectra during the gas exchange process at 5 wt% D_2O.

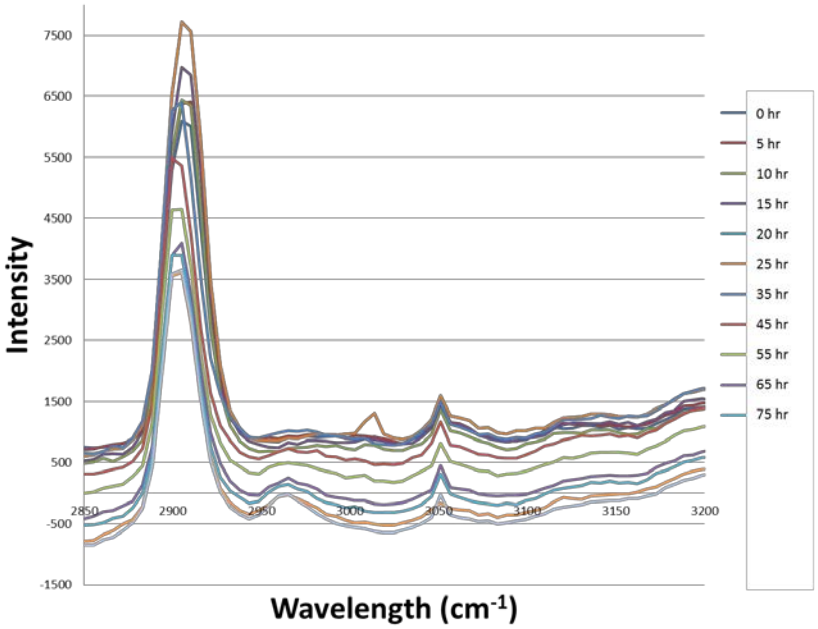

Figure 12: Variation of Raman spectra during the gas exchange at 50 wt% D_2O.

Subtask 4.2 Gas Exchange Kinetics Measurements in the Presence of Free Water

CO_2 (l)-CH_4 exchange kinetics in batch mode:

- The sand (120 μm) of 52.9 g moistened with water of 4.9 g was packed into a high-pressure vessel to yield the porosity of 36% and water saturation (S_W) of 45% in pore space. Hydrate formation was initiated by pressurizing the vessel with pre-cooled methane gas up to 7.4 MPa at isochoric condition. After the hydrate formation reaction was completed, CH_4 gas was discharged until the pressure in the system reached 4.21 MPa, at which hydrate will be unstable and start dissociating. The pressure increased to near phase equilibrium pressure of 4.86 MPa for the CH_4 hydrate-liquid water-vapor system, as a result of the hydrate dissociation. The mass balance calculation demonstrates the hydrate saturation (S_H) of 33% and free water saturation (S_{FW}) of 14%. CO_2 gas was injected into the reactor under the constant flow rate mode of 15 ml/min while the pressure in the reactor was maintained at 3.59 MPa at 1°C, respectively, to allow the removal of CH_4 gas in head and pore spaces. When the composition of CH_4 in the gas flow coming out of the reactor became lower than 2%, CO_2 was further pressurized to 5.4 MPa to create CO_2 (l) stable condition. When the pressure reached 5.4 MPa, all valves were closed to allow the gas exchange reaction to be carried out in isochoric condition. After 717 hours from the beginning of gas exchange, the mixture of [CO_2 (l)-CH_4] in head space was expanded to a 500 ml empty chamber to turn [CO_2 (l)-CH_4] to [CO_2 (g)-CH_4]. Thus, the gas sample collected from the chamber was homogeneously mixed and could represent the composition of head space. A gas sample was collected from [CO_2 (g)-CH_4] in the chamber for GC analysis. The gas composition in gas phase was measured by using a Shimadzu DS2014 gas chromatograph with a thermal conductivity detector (TCD) detector and He carrier gas.
- The gas sample collected from the homogenously mixed gases shows 1.38% of CH_4 mole composition in CO_2 (l). The exchange efficiency and gas recovery rate for the CO_2 (l) + CH_4 system was estimated based on gas composition collected in the chamber after the gas exchange process was completed. The CH_4 recovery rate reached 52% after 717 hours from the beginning of the exchange process (Figure 13).
- The recovery rate of CO_2 (l)-CH_4 exchange is compared with CO_2 (g)-CH_4 and [CO_2 +N_2]-CH_4 exchange under free water condition (Table 2). Figure 13 shows that the CH_4 recovery rates of CO_2 (l)-CH_4 exchange is larger than that of CO_2 (g) + CH_4 under free water condition and similar with CO_2 (g)-CH_4 exchange under no free water condition. Larger recovery rates would be explained by larger fugacity of CO_2 (l). It is believed that the replacement of CH_4 with CO_2 molecules in CH_4 hydrate phase occurs in high extent under high CO_2 fugacity condition, though free water or hydrate formed from free water readily blocks the pathway of CO_2 for accessing CH_4 hydrate.

CO_2 (l)-CH_4 and [CO_2 + N_2]-CH_4 exchange kinetics in column mode:

- A high-pressure, tri-axial vessel was used for CO_2 (l)-CH_4 and [CO_2 + N_2]-CH_4 exchange kinetics in column mode. The sediment conditions for gas exchange experiments are listed in Table 2. Hydrate formation was initiated by pressurizing the vessel with methane gas up to 7.7 MPa at 6°C until no volume change was observed. After the hydrate formation reaction was completed, CH_4 gas was discharged until the pressure in the system reached 1.26 MPa for partial dissociation of CH_4 hydrate.

The pressure increase was used for calculating the free water amount released from the hydrate by using the equation of state.

- CH_4 trapped in the pore space was flushed with CO_2 (g) and [CO_2 + N_2] mixed gas at a constant flow rate of 10 ml/min, while the pressure in the vessel was maintained at 3.5 and 9.1 MPa for CO_2-CH_4 and [CO_2 + N_2]-CH_4 exchanges, respectively. When 5 pore-volumes of fluids were injected into the vessel, it was assumed that the commencement of the gas exchange process, as the composition of CH_4 in effluent, was below 0.1 %. For CO_2 (l)-CH_4 exchange, the vessel was pressurized up to 6.2 MPa with liquid CO_2. The injection rates of CO_2 (l) and [CO_2 + N_2] mixed gas were 0.033 ml/min during the gas exchange process, and the mixture of [CO_2 (l) + CH_4] and [CO_2 + N_2+ CH_4] was discharged by a syringe pump at constant pressure of 6.2 and 9.1 MPa, respectively. The effluent was collected from the middle of the discharge line for analysis of CH_4 composition.
- Previous batch results showed that the injection of CO_2 (l) instead of CO_2 (g) or [CO_2 + N_2] mixed gas enhances the recovery rate, despite the presence of free water in pore space (Figure 13). The gas exchange test was also carried out in column mode to examine the efficiency of CH_4 production in continuous flow operation. The effluent mixture from the vessel was collected for analysis of gas composition during gas exchange reaction. The resulting CH_4 composition was converted to the amount of CH_4 mole in a unit volume of effluent stream. Figure 14 shows that the CH_4 amount produced in the CO_2 (l)-CH_4 exchange is larger than that in the [CO_2 + N_2]-CH_4 exchange. CO_2 injection allows the CO_2 (l)-CH_4 exchange reaction to occur in the gas hydrate reservoir since CO_2 exists in liquid form in the CH_4 hydrate stability zone. The CO_2 (l)-CH_4 exchange showed a higher recovery rate of CH_4 under free water condition compared to the [CO_2 + N_2]-CH_4 exchange. This result implies that CO_2 (l) with high driving force could be used for efficient CH_4 production in column mode under free water condition.
- The team compared CO_2 (l), instead of CO_2 (g), with [CO_2 + N_2] mixed gas in the column operation to verify the feasibility of the CO_2-CH_4 exchange in continuous flow type productions. The column operation showed a higher amount of CH_4 in effluent flow, which would accompany a higher total recovery rate, as seen in batch operation. Thus, the CO_2 (l)-CH_4 exchange would be a better option for continuous CH_4 productions than the [CO_2 + N_2]-CH_4 exchange.

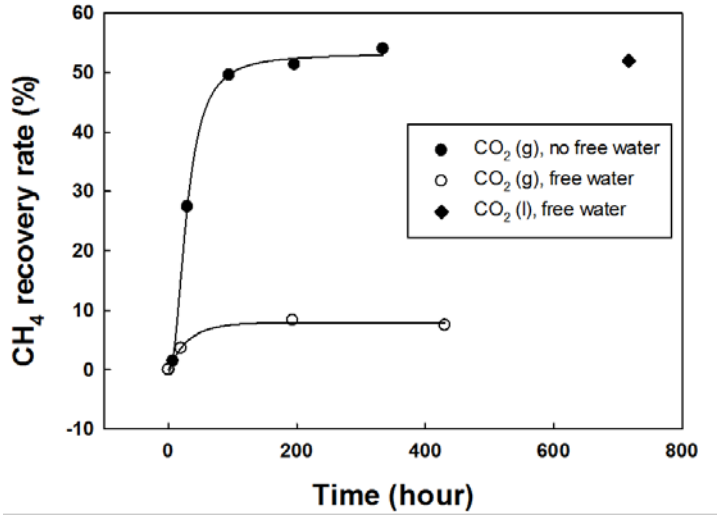

Figure 13: CH_4 recovery rate in CO_2-CH_4 gas exchange system in batch mode.

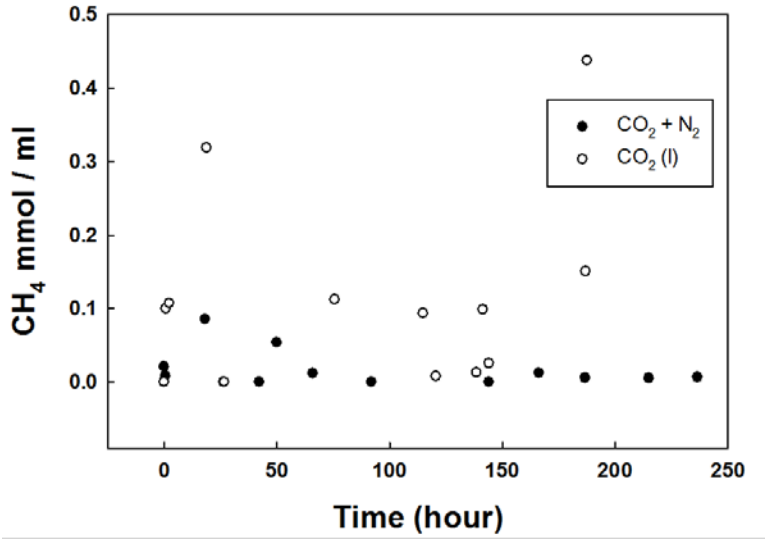

Figure 14: The composition of CH_4 gas in the effluent discharged from the vessel.

Table 2: Experimental conditions of gas exchange in MHBS.

Type	Feed Fluid	Sand (g)	Water (g)	Porosity (%)	S_W (%)[a]	S_H (%)	S_{FW} (%)[b]	Initial CH_4 Composition (%)
batch	CO_2 (l)	52.7	4.9	36	45	33	14	0.1
batch	CO_2 (g)	53.7	3.9	37	32	34	–	2.1
batch	CO_2 (g)	53.4	5.0	38	41	31	13	1.4
column	CO_2 (l)	263.2	25.6	38	43	32	14	0.0
column	CO_2+N_2	265.0	25.9	37	44	33	15	0.1

[a] Initial water saturation in sand pore before CH_4 hydrate formation.
[b] Free water saturation dissociated from CH_4 hydrate in sand pore.

Subtask 4.3 Data Exchange and Comparative Analysis of Gas Exchange Rates at Various Conditions

Due to the unavailability of gas exchange data from other national laboratories, this task could not be performed as planned. Nothing to report for this period.

Task 5.0 Pore Scale Visualization and Characterization of Hydrate-Bearing Sediments

Subtask 5.1 Pore Scale Visualization of Hydrate-Bearing Sediments with High Resolution X-ray CT Scanners

Identified the optimum scanning parameters: SSD = -50 mm, DSD = 30mm, exposure time = 16 sec for 10x lens with 1.694 µm pixel resolution or 6 sec for 4x lens with 4.2183 µm pixel resolution.

Analog studies: sand + water + polyurethane spheroids, as shown in Figure 15.

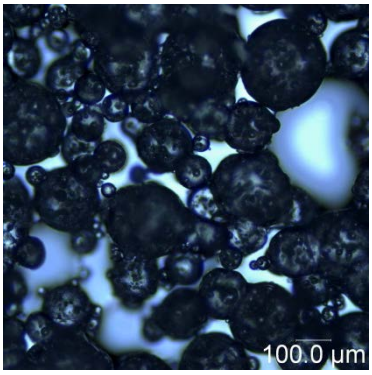

(a) Microscopic photos of polyurethane spheroids used as hydrate analogues.

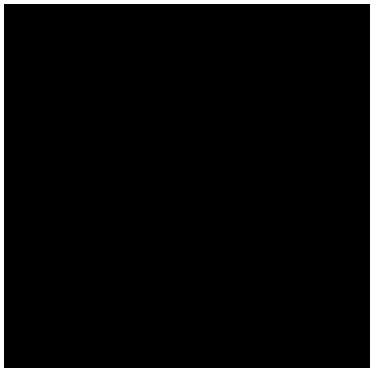

(b) The 3D CT images of dried polyurethane spheroids.

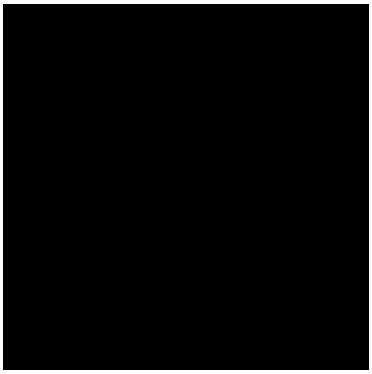

c) A slice view of the analogue specimen with pixel resolution of 0.592 µm.

(d) The CT image processing for phase separation (blue: sand particles; green: water; white: polyurethane spheroids; black: air).

Figure 15: Analogue specimen.

Using a Be vessel has the potential for pore-scale visualization of hydrate bearing sediments (Figure 16). The low atomic number of Beryllium ($Z = 4$) makes it the perfect material for high-pressure core holders used in X-ray CT scanning.

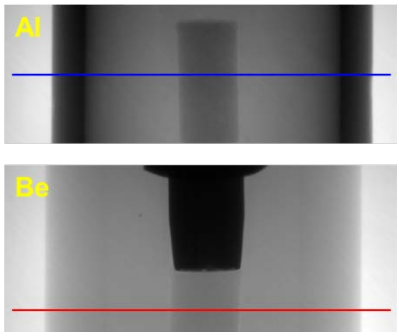

(a) Projection of quartzitic sands in the Al and Be core holders. Notice that the wall thickness of the Al core holder is about half of that of the Be core holder.

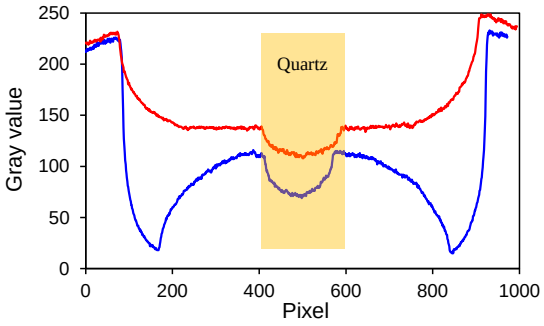

(b) Corresponding grey value profiles in (a). Al core holder absorbs much more X-rays than the Be vessel. Obtained slice view of CT images using (c).

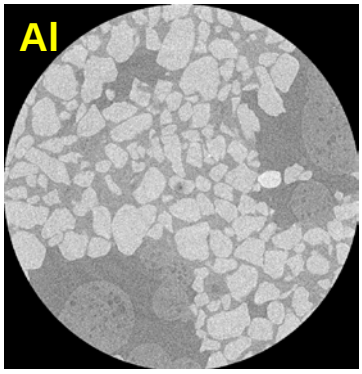

(c) The aluminum core holder.

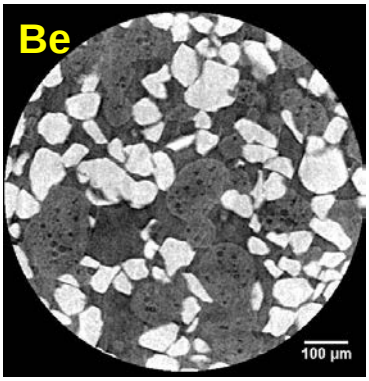

(d) The Be core holder.

Figure 16: The 3D micro-XCT scans of analogue specimens using aluminum (Al) and beryllium (Be) core holders. The image resolution is 0.592 µm/pixel. The CT images obtained using the Be vessel have better phase contrast with less image noises and artifacts.

The dependency of CT numbers on the scanning voltage varies with materials. Therefore, different composites within the specimen show different gray value distribution under various scanning voltages (Figure 17). The simple average of the two slice images obtained at two photon energy levels led to one image with more phase contrast and less noises.

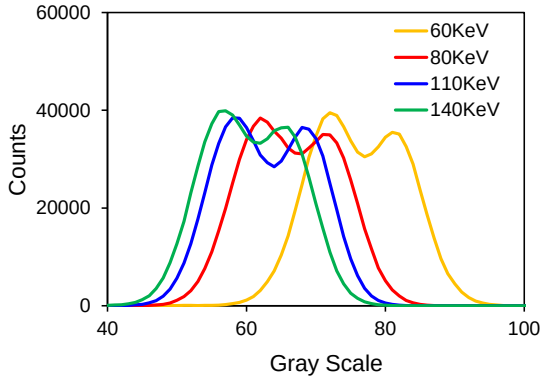

(a) Gray scale distributions obtained at four different scanning energy levels. Lower scanning energy levels (when other scanning conditions remain identical) render brighter images (higher CT numbers) with slightly higher contrast among different composites.

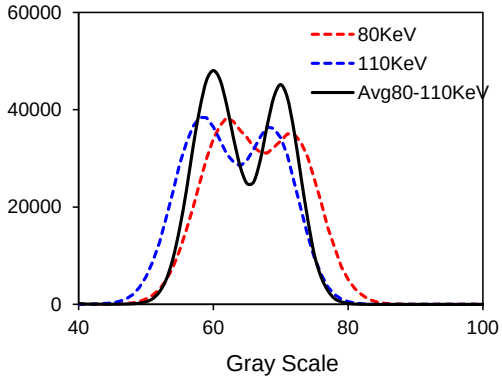

(b) The gray scale distribution of averaged images from two scanning energy levels has much sharper contrast with less noise scattering.

Figure 17: Gray scale (CT number) distribution of the analogue specimen.

The peripheral pressure-temperature systems for the beryllium core holder have been setup. The low-temperature, high-pressure fluid circulation system was tested. Heat shrink tubing was used to wrap the Be vessel, serving as both a temperature insulation layer and an air barrier to prevent moisture condensation outside of the Be vessel. The image in Figure 18 shows the high-pressure Be vessel connected with flexible PEEK tubing sitting on the micro-CT station.

Figure 18: High-pressure beryllium chamber on the micro-CT station.

The Paganin's single distance algorithm was implemented to suppress phase-contrast artefacts and improve phase separation. This will be beneficial to identify the hydrate phase from the water phase in CT images, which has long been a challenge as the densities of these two phases are very close. Also, the CT system and peripheral components are ready to synthesize hydrate bearing sediments in the beryllium vessel.

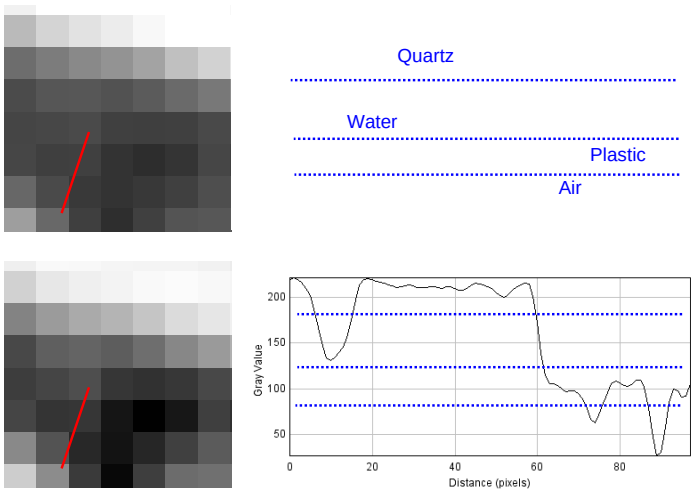

Figure 19: Slice view and gray value profiles before (top) and after (bottom) using the Paganin's single distance algorithm for CT image processing.

This technique (Figure 20) is applied for processing CT images of partially water-saturated sands specimen obtained using the NETL micro-CT, as shown in Figure 19.

(a) Slice view of the unsaturated sands.

(b) Corresponding gray value profile for the air, water, and quartz phases (after implementing the Paganin's single distance algorithm to obtained CT images).

(c) The 3D view of processed CT images of partially water-saturated sands.

Figure 20: Scanning of unsaturated sands using NETL micro-CT.

To advance the grain-scale modeling of flow based on 3D CT images, fine quartztic sands (F110) were scanned using a microfocus X-ray CT (Figure 21). The corresponding pore structure was extracted from these CT images using the rolling-ball algorithm. The F110 was selected because experimental data of their fundamental physical and hydrological properties, such as grain size distribution and permeability, were available. These data can be later used to validate our numerical simulation results.

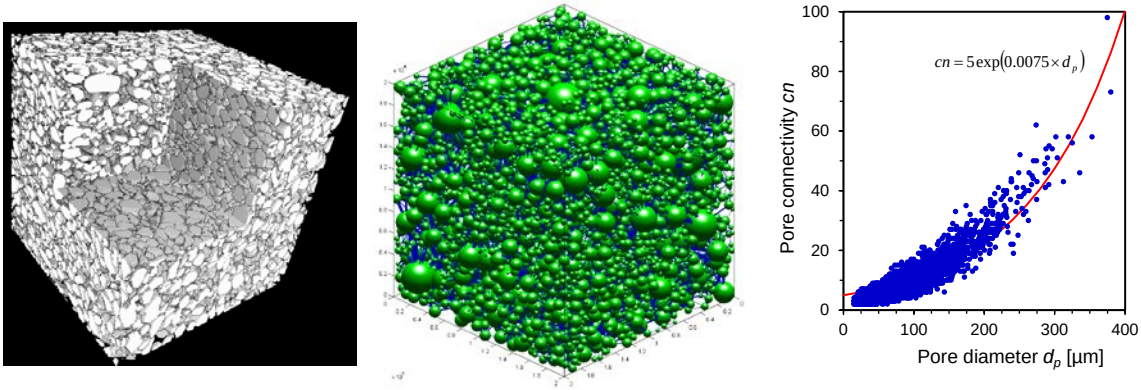

(a) 3D micro-CT images of a 2cm×2cm×2cm F110 sand sample, with pixel resolution of 4.22 micron.

(b) Extracted pore network structure from the CT image. The green bubbles represent the pores and their volume is scaled to the bubble size. The blue lines represent the throat connecting neighboring pores and the line thickness reflects the pore throat size.

(c) Fundamental statistics of pores in fine sands based on CT images: pore connectivity increases exponentially with pore diameter. The scanned sample has a mean grain size of 118 μm, mean pore radius 36.1 μm, and average pore connectivity 7.95 (i.e., each pore is connected with 7.95 neighboring pores on average).

Figure 21: Pore structure extraction from CT images and fundamental pore characteristics.

Subtask 5.2 Grain Scale Constitutive Modeling for Hydrate-Bearing Sediments

Figure 22 shows capillary tube models: effects of hydrate pore habits on pipe flow.

Pore-filling (annulus flow)		Grain-coating (pipe flow)		
				
Circular cross section	Simple cubic packing	Circular cross section	Simple cubic packing	Simple cubic packing + Capillary effect

(a) Hydrate pore habit effects are studies using capillary tube model but with five different cross sectional geometries. Note: (1) blue represents hydrate crystals and gray represents grain particles; (2) two cross sectional shapes are considered: circular and simple cubic packing of monosized grains.

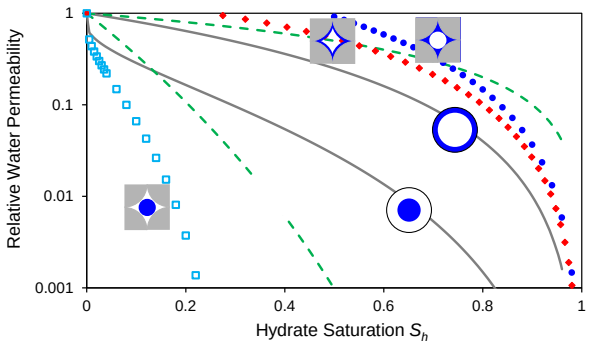

(b) Based on modified Hagen-Poisuille and annulus flow equations considering hydrate nucleation in changing tube cross sectional area, the team obtained information on how hydrate formation reduces water permeability for five different pore habits in (a).

Figure 22: Water permeability reduction due to hydrate: effects of hydrate pore habits.

In general, pore-filling type hydrates are more disruptive than grain-coating hydrates in water flow through hydrate bearing sediments, due to increased hydrate-water contact area (Figure 22). For example, a hydrate saturation Sh = ~0.1 for pore-filling hydrates in simple cubic packing case can reduce relative water permeability to 0.1, but requires Sh = ~0.8 of grain-coating hydrate in simple cubic packing case to cause such a drop in water permeability.

Figure 23 shows the 2D lattice pore network modeling: effects of hydrate distribution on the hydraulic properties of hydrate bearing sediments.

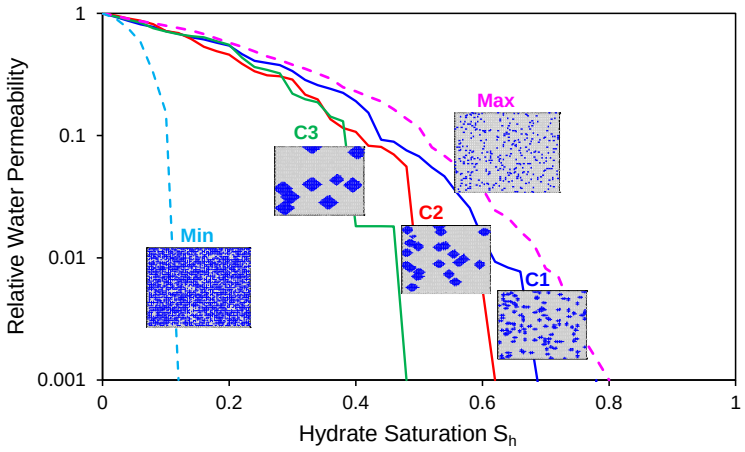

Figure 23: Water permeability reduction due to hydrate: effects of heterogeneous hydrate distribution.

Figure 23 shows five hydrate nucleation preferences are considered in this study: preferential nucleation in the largest (Max) or the smallest (Min) pores, or in clusters but with different cluster sizes (C1, C2, and C3 with increasing hydrate cluster size). Five insects in the above figure show hydrate distribution according to these five accumulation habits with identical hydrate saturation of Sh = 0.2. Results suggest that the cases of hydrate clogging in the largest (Max) and smallest (Min) pores provide bounds for effects on water permeability reduction due to an increase in hydrate saturation. When hydrate forms in clusters or patches (C1, C2, and C3), a larger cluster size (C3) is more disruptive to flow, which agrees with published FEM simulation results.

Figure 24 shows the formation of hydrate makes the main flow path more tortuous.

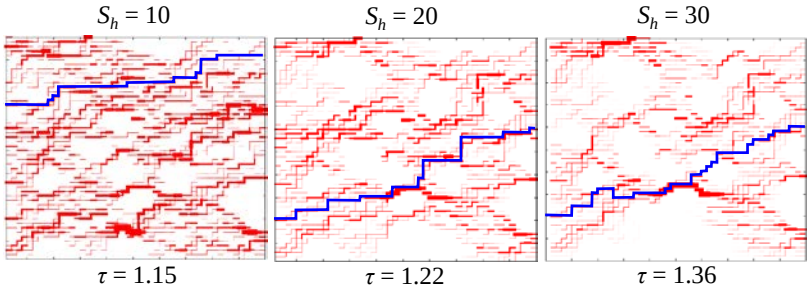

(a) Fluid fluxed (red tubes) and the critical flow path (blue tubes) across the pore network. Here, the critical flow path is defined as the percolation path that carries the most amount of flux across the network.

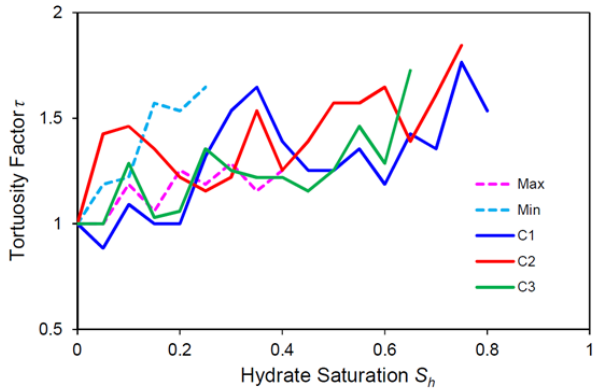

(b) The dependency of flow tortuosity on hydrate saturation is not monotonic. For each hydrate distribution pattern (see Figure 23b), tortuosity oscillates and each decrease in tortuosity corresponds to a shift to another critical flow path.

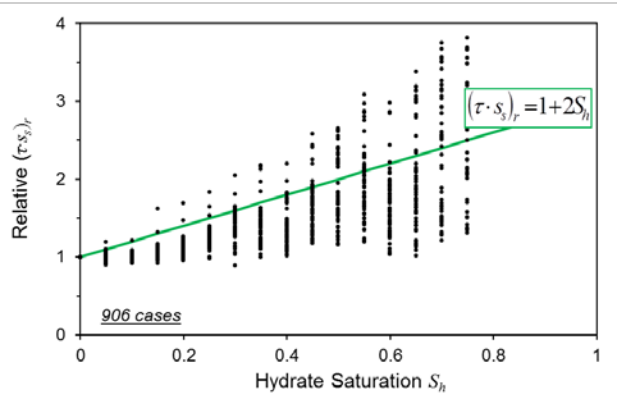

(c) As a general trend, flow tortuosity increases with increasing hydrate saturation. The relative tortuosity is compared with hydrate-free network. In total, 906 realizations of networks with various hydrate saturations and random distributions are studied.

Figure 24: Hydrate effect on fluid flow tortuosity in hydrate bearing sediments.

Based on the studies of the effect of hydrate on flow tortuosity, the team developed the relationship between the apparent water permeability in hydrate bearing sediments and hydrate saturation using modified Kozeny-Carman equation.

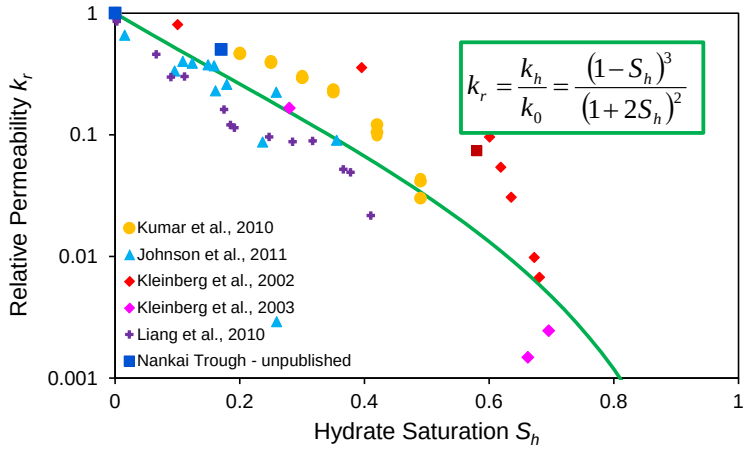

Figure 25: Comparison of prediction based on the new relative permeability relations with literature data.

Based on pore network modeling investigations on hydrate effects on flow tortuosity and sediment specific surfaces, the semi-empirical Kozeny-Carman (KC) equation can be updated by considering hydrate effects on water flow processes in sediments (Figure 25). According to the KC equation, water permeability is proportional to sediment porosity ϕ and inversely proportional to flow tortuosity τ and soil specific surface s_s: $k = c\phi/(\tau \times s_s)^2$, where c is a constant. When hydrate nucleates in sediment pores, the porosity becomes $\phi_h = \phi_0(1-S_h)$; tortuosity and specific surface becomes $(\tau \times s_s)_h = (\tau \times s_s)_0(1+2S_h)$ based on pore network modeling results of a statistic mean of 906 cases considering different hydrate saturations, random distributions, and hydrate cluster sizes. Therefore, the reduction in water permeability as a function of hydrate saturation becomes: $k_r = (1-S_h)^3/(1+2S_h)^2$. This model was developed based on the KC equation, which captures the essential physics of water flow in porous media. It can predict the kr-Sh trend well, according to few available laboratory/field measurements (shown above). Additionally, this model have no other variables as the widely used Tokyo model: $k_r = (1-S_h)^N$, where results can vary dramatically depending on which N value is used (see Figure 22b). Therefore, it is more convenient to implement current numerical simulators to study the flow behavior of hydrate bearing sediments.

Figure 26 shows the 3D extracted pore network based on X-ray CT images and corresponding simulations.

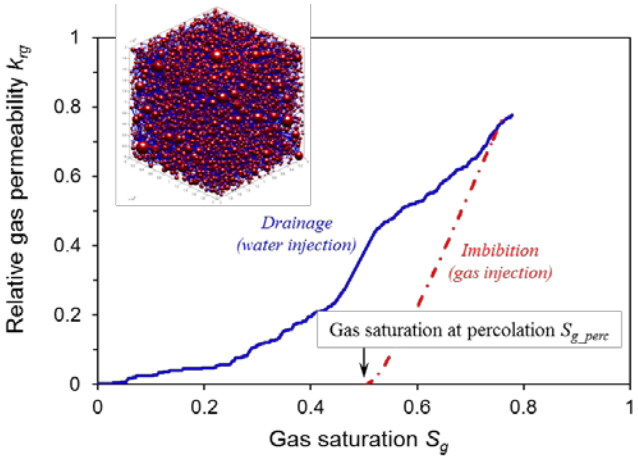

Figure 26: Hysteresis of relative gas permeability during drainage and imbibition processes using 3D pore network extracted from CT images of F110 sands.

Hydrates_FY15

Task 1.0 – Project Management and Outreach

The Hydrates FY15 FWP was delivered to SCNGO on July 9, 2014.

The Hydrates FY15 PMP was delivered to SCNGO on July 30, 2014.

Task 2.0 Reservoir Simulation of Gas Hydrates Production Field Tests

Subtask 2.1 Alaska North Slope Production Test Simulation Assistance

For October, the effect of horizontal production wells on Site 2 (deeper version of Mt. Elbert model) was investigated. An improvement on this model being is being developed with wellbore refinements in all hydrate-bearing layers. Long term simulations will be carried out with/without wellbore heating to better understand model performance.

Subtask 2.2 International Code Comparison Continuation – Iġnik Sikumi History Match Analysis and Marine Deposit Based on the 2013 Nankai Trough Test or Other Marine Sites

Numerical simulations, using the Mix3HydrateResSim (Mix3HRS) simulator, were executed to model injections of gaseous CO_2 into a 2D reservoir domain which is inclined at an angle of 25 degrees with the horizontal. It is modeled inclined to simulate the formations at the Prudhoe Bay L-Pad region (particularly C-Sand formations) situated in the North Slope, Alaska.

Task 3.0 Laboratory Hydrologic and Geomechanical Characterization and Analysis of Hydrate-Bearing Sediments

Subtask 3.1 Laboratory Measurement of Relative Permeability of CH_4 Gas in Brine-Saturated Hydrate-Bearing Sediments

Relative permeability of CH_4 gas in hydrate bearing sediments is a key parameter for numerical simulations and is yet to be determined with relevant samples. This task will build a new experimental setup to measure the relative permeability based on existing mobile carts.

- The literature review is in progress.
- Preliminary test setup was designed. Test equipment and parts were ordered accordingly.
- A plan for improving the existing temperature chamber was proposed. The temperature chamber will accommodate our mobile cart so the test can be conducted under better control of temperature (less temperature fluctuation).

Subtask 3.2 Tri-Axial Compression Tests on Hydrate-Bearing Sediments with Induced Hydrate Dissociation under Shear Stress

Compression tests have been completed on hydrate bearing sediments in FY14. Comprehensive geomechanical tests will be completed by using the measurement during hydrate dissociation. This task is designed to perform the tri-axial compression tests during hydrate dissociation.

- The literature review is in progress.
- A plan for improving the existing temperature chamber was proposed for the test to be conducted under better control of temperature (less temperature fluctuation).

Subtask 3.3 Methodology Developments for Modeling Geomechanical Stability of Hydrate-Bearing Sediments under Hydrate Dissociation Condition

Effort has not begun on this subtask; pending supporting research staff emplacement.

Task 4.0 Pore-Scale Visualization and Characterization of Hydrate-Bearing Sediments

Subtask 4.1 Effect of Continuous Brine Flow on Hydrate Formation and Dissociation Behaviors

Methane hydrates was formed in pure silica sands using the Be-vessel and high resolution CT images (4.2 micron/pixel) were obtained before hydrate formation, after hydrate formation, and after hydrate dissociation. Modification of pressure and flow controls to allow brine circulation within the synthesized hydrate bearing sediments is underway.

Subtask 4.2 Water and Gas Distributions after Hydrate Dissociation and Implications to Permeability

Effort has not begun on this subtask; pending completion of Subtask 4.1.

Subtask 4.3 Links between Hydrate Morphologies and Geomechanical Properties

Effort has not begun on this subtask; pending completion of Subtask 4.1.

Subtask 4.4 Microfluidic-Based Permeability of Hydrate-Bearing Sediments

Designing and constructing the Methane Hydrate formation apparatus is underway. This activity involved specifying and purchasing instruments and equipment for the apparatus, as well as fabricating the electrical, process flow, and mechanical aspects of the apparatus.

Forecast for Next 6 Months

Hydrates_FY15

Task 1.0 – Project Management and Outreach

Submit the Hydrates FY14-Q4 Quarterly Progress Report and a briefing will be scheduled with SCNGO in November 2014.

Submit the Offshore FY15-Q1 Quarterly Progress Report on January 30, 2015.

Task 2.0 Reservoir Simulation of Gas Hydrates Production Field Tests

Subtask 2.1 Alaska North Slope Production Test Simulation Assistance

The next six months will involve carrying out uncertainty and sensitivity analyses on both the L-Pad and Mt. Elbert models. Field data will be continuously incorporated into the heterogeneous models as they become available. Also, detailed wellbore design and flow assurance studies will be conducted to forestall problems associated with reformation of hydrates within the wellbore during production. This will involve the application of computational fluid dynamics; its results will be coupled with reservoir models.

Subtask 2.2 International Code Comparison Continuation – Iġnik Sikumi History Match Analysis and Marine Deposit Based on the 2013 Nankai Trough Test or Other Marine Sites

Various numerical simulations will be performed using different production techniques to investigate how the reservoir parameters change for each technique, particularly for the geologic formations with high-hydrate saturations. Focus will change from injecting gaseous CO_2 into different reservoir domains to injecting liquid CO_2 by modifying the Mix3HRS code.

Task 3.0 Laboratory Hydrologic and Geomechanical Characterization and Analysis of Hydrate-Bearing Sediments

Subtask 3.1 Laboratory Measurement of Relative Permeability of CH_4 Gas in Brine-Saturated Hydrate-Bearing Sediments

- The literature review will be continued. (FY15-Q1)
- Experimental methodology for the relative measurements will be developed. (FY15-Q1)
- The temperature chamber will be ready for the test by adding new gas lines, temperature controller, and gas detectors. (FY15-Q2)
- New equipment and parts will be assembled into the mobile cart. (FY15-Q2)
- The experimental method and test setup will be examined by conducting preliminary tests. (FY15-Q2)

Subtask 3.2 Tri-Axial Compression Tests on Hydrate-Bearing Sediments with Induced Hydrate Dissociation under Shear Stress

- The literature review will be continued. (FY15-Q1)
- A reasonable strategy of hydrate dissociation will be established in consideration of actual HBS conditions anticipated during field production tests. (FY15-Q1)
- An overall test plan will be provided. (FY15-Q1)
- An initial compression test will be conducted, simultaneously examining the test plan and setups. (FY15-Q2)

Subtask 3.3 Methodology Developments for Modeling Geomechanical Stability of Hydrate-Bearing Sediments under Hydrate Dissociation Condition

Effort has not begun on this subtask; pending identification of research staff on the task. The team hopes to validate the constitutive model with experimental data on the modeling of dissociation on stress-strain behavior. The team would also conduct and develop benchmark tests for validating the coupling analysis for geomechanics analysis of operational scenarios, for use in such cases as methane extraction from the ground.

Task 4.0 Pore-Scale Visualization and Characterization of Hydrate-Bearing Sediments

Subtask 4.1 Effect of Continuous Brine Flow on Hydrate Formation and Dissociation Behaviors

Brine flows through hydrate bearing reservoirs increasing salt concentration that shifts the hydrate stability condition. This is a potential mechanism of methane vents piercing through hydrate stability zones and is also relevant to the non-cementing hydrate recipe developed at NETL. The team intends to investigate such a process using the Be core holder and 2D microfluidic models, which enables us to directly visualize the changes in hydrate pore habits and morphologies during continuous brine flow through the synthesized hydrate bearing sediments.

Subtask 4.2 Water and Gas Distributions after Hydrate Dissociation and Implications to Permeability

Water and gas permeability are critical to economic gas production from hydrate bearing reservoirs. Characterization of the dynamic process during hydrate dissociation has not been well investigated. The team plans to deploy the micro-CT and high-pressure 2D microfluidic models to investigate the water/gas migrations during hydrate dissociation. Results are expected to shed light on the relative water and gas permeability during gas production.

Subtask 4.3 Links between Hydrate Morphologies and Geomechanical Properties

The Be vessel is modified to be equipped with acoustic wave measurement capability. The wave velocity results combined with concurrent CT images of hydrate distribution within sediments can enhance the understanding of hydrate morphology effects on measured wave speed. This may offer new interpretations of existing laboratory wave data.

Subtask 4.4 Microfluidic-Based Permeability of Hydrate-Bearing Sediments

Activity will be focused on bringing the apparatus online and testing its functionality. The first experiment will be to form THF (tetrahydrofuran) Hydrate in the apparatus and record the formation with digital imaging. These images will be interpreted to discover the formation characteristics of THF Hydrate. The apparatus will also be used to determine the permeability, hydrate saturation, and susceptibility to develop manipulation through thermodynamic input.

Products

Publications, Conference Papers, and Presentations

Cha, J., and Seol, Y., "Formation Kinetics of Gas Hydrates Incorporated with Additives and Their Industrial Applications," Gordon Research Conference, Natural Gas Hydrate, Galveston, TX, March 24 – 28, 2015. (Subtask 4.1)

Choi, J., Cha, J., Dai, S., and Seol, Y., "Laboratory Formation of Non-Cementing Hydrates in Sandy Sediments," *Geochemistry, Geophysics, Geosystems*, Volume 15, Issue 4, p. 1648-1656, 2014. (Subtask 3.1)

Dai, S., and Seol, Y., "Water Permeability in Hydrate-Bearing Sediments: A Pore-Scale Study," *Geophysical Research Letters*, Volume 41, Issue 12, p. 4176-4184, 2014. (Subtask 5.2)

Dai, S., Seol, Y., and Santamarina, C., "Effects of Hydrate on Physical Properties of Hydrate Bearing Sediments: Pore Scale Studies," Gordon Research Conference, Natural Gas Hydrate, Galveston, TX, March 24-28, 2015. (Subtask 5.1)

Lin, J-S, Seol, Y., and Choi, J.,"An SMP Subloading Critical State Model for Methane Hydrate-Bearing Soils," *International Journal for Numerical and Analytical Methods in Geomechanics*, Manuscript NAG-14-0044, submitted on March 2, 2014 (resubmission). (Subtask 3.2)

Seol, Y., Choi, J., and Dai, S., "Multi-Properties Characterization Chamber for Hydrate Bearing Sediments," *Review of Scientific Instruments*, Volume 85, Issue 8, 084501, 2014; http://dx.doi.org/10.1063/1.4892995. (Subtask 3.1)

Wickramanayake, S., Hopkinson, D.S., Feng, J., Hong, L., Zeh, M., Plasynski, D., Seol, Y., Myers, C., and Luebke, D., "Mechanically Robust Hollow Fiber Supported Ionic Liquid Membranes for CO_2 Separation Applications," *Energy and Environmental Science*, Manuscript ID EE-ART-03-2014-000909, accepted on July 10, 2014. (Subtask 5.1)

Yoon, R.J., Wang, R., Wang, Z., Seol, Y., "Effect of Hydrophobic Surfaces on the Kinetics" *ACS-Journal of Chemical Engineering Data (JCED)* Special Issue in Honor of E. Dendy Sloan, accepted on Sep 23, 2014 (Subtask 4.1)

Websites or Other Internet Sites

Hydrate research activity was featured in *Researchnews*, October 2014, Issue 1, p. 3, "Revealed Secrets in Locked in ICE" and "NETL In-House Research Program: Natural Gas Hydrate R&D" page http://www.netl.doe.gov/File%20Library/Library/Newsroom/researchnews/Research_News_October2014_101514.pdf

Technologies or Techniques

Nothing to report during this period.

Inventions, Patent Applications, and Licenses

Nothing to report during this period.

Other Products

Nothing to report during this period.

Changes/Problems

The delayed selection of a long-term depressurization test and collection of relevant dataset resulted in a delay in task progress. A no cost-extension was requested to November 14, 2014. (Task 2.0)

Mechanical tests with the CO_2 hydrate test were completed in September 2014. (Task 3.0)

The exchange mechanism test was completed in September 2014. (Task 4.0)

Appendix A: Participating and Other Collaborating Organizations

This list includes the name and organization of all federal, URS, university, and ORISE participants. Each quarter, changes or additions will be shown in highlighted yellow text.

Natural Gas Hydrates Research Portfolio Participating and Other Collaborating Organizations (Hydrates_2013.07.02)

Task/Subtask/Sub-subtask Number – Name	Name	Organization
Task 1.0 – Project Management and Outreach		
Subtask 1.1 – PMP	Gary Sames Yongkoo Seol	NETL-ORD
Subtask 1.2 – Meetings	Yongkoo Seol	NETL-ORD
	Jeffery Ilconich	URS
Subtask 1.3 – Reports	Gary Sames Yongkoo Seol	NETL-ORD
	Jeffery Ilconich	URS
Subtask 1.4 – RES Management Support	Jeffery Ilconich	URS
Subtask 1.5 – Outreach	Yongkoo Seol	NETL-ORD
	Jeffery Ilconich	URS
Subtask 1.6 – Portfolio Management	Yongkoo Seol	NETL-ORD
	Jeffery Ilconich	URS
Task 2.0 – Reservoir Simulation of Gas Hydrates Production Field Tests		
Subtask 2.1 – Simulations of Long-Term Production Scenarios: Depressurization and CO_2 Exchange	Yongkoo Seol	NETL-ORD
	Brian Anderson	RUA-WVU
Subtask 2.2 – International Code Comparison Problem Set Based on Iğnik Sikumi	Yongkoo Seol	NETL-ORD
	Brian Anderson	RUA-WVU
Task 3.0 – Developing Constitutive Models of Various Hydrate-Bearing Sands		
Subtask 3.1 – Laboratory Measurements of Geomechanical Strength and Deformability	Yongkoo Seol	NETL-ORD
	Jeong-Hoon Choi	ORISE
Subtask 3.2 – Developing Constitutive Models of Various Hydrate-Bearing Sands	Yongkoo Seol	NETL-ORD
	Jeen-Shang Lin	RUA-PIT
Task 4.0 – Assessment of Gas Exchange Processes of CH_4 Hydrate with CO_2 under Reservoir Conditions		
Subtask 4.1 – Gas Exchange Mechanism with Raman Spectroscopy	Yongkoo Seol	NETL-ORD
	Jong-Ho Cha	ORISE

Task/Subtask/Sub-subtask Number – Name	Name	Organization
Subtask 4.2 – Gas Exchange Kinetics Measurements in the Presence of Free Water	Yongkoo Seol	NETL-ORD
	Jong-Ho Cha	ORISE
Subtask 4.3 – Data Exchange and Comparative Analysis of Gas Exchange Rates at Various Conditions	Yongkoo Seol	NETL-ORD
	Jong-Ho Cha	ORISE
Task 5.0 – Pore Scale Visualization and Characterization of Hydrate-Bearing Sediments		
Subtask 5.1 – Pore Scale Visualization of Hydrate-Bearing Sediments with High Resolution X-ray CT Scanners	Yongkoo Seol	NETL-ORD
	Sheng Dai	ORISE
Subtask 5.2 – Grain Scale Constitutive Modeling for Hydrate-Bearing Sediments	Yongkoo Seol	NETL-ORD
	Sheng Dai	ORISE

Natural Gas Hydrates Research Portfolio Participating and Other Collaborating Organizations (Hydrates_FY15)

Task/Subtask/Sub-subtask Number – Name	Name	Organization
Task 1.0 – Project Management and Outreach		
Subtask 1.1 – PMP	Gary Sames Yongkoo Seol	NETL-ORD
Subtask 1.2 – Meetings	Yongkoo Seol	NETL-ORD
	Jeffery Ilconich	URS
Subtask 1.3 – Reports	Gary Sames Yongkoo Seol	NETL-ORD
	Jeffery Ilconich	URS
Subtask 1.4 – RES Management Support	Jeffery Ilconich	URS
Subtask 1.5 – Outreach	Yongkoo Seol	NETL-ORD
	Jeffery Ilconich	URS
Subtask 1.6 – Portfolio Management	Yongkoo Seol	NETL-ORD
	Jeffery Ilconich	URS

Task/Subtask/Sub-subtask Number – Name	Name	Organization
Task 2.0 – Reservoir Simulation of Gas Hydrates Production Field Tests		
Subtask 2.1 – Alaska North Slope Production Test Simulation Assistance	Yongkoo Seol	NETL-ORD
	Taiwo Ajayi Prathyusha Sridhara	ORISE
Subtask 2.2 – International Code Comparison Continuation – Iġnik Sikumi History Match Analysis and Marine Deposit Based on the 2013 Nankai Trough Test or Other Marine Sites	Yongkoo Seol	NETL-ORD
	Taiwo Ajayi Prathyusha Sridhara	ORISE
Task 3.0 – Laboratory Hydrologic and Geomechanical Characterization and Analysis of Hydrate-Bearing Sediments		
Subtask 3.1 – Laboratory Measurement of Relative Permeability of CH_4 Gas in Brine-Saturated Hydrate-Bearing Sediments	Yongkoo Seol	NETL-ORD
	Jeong-Hoon Choi	ORISE
Subtask 3.2 – Tri-Axial Compression Tests on Hydrate-Bearing Sediments with Induced Hydrate Dissociation under Shear Stress	Yongkoo Seol	NETL-ORD
	Jeong-Hoon Choi	ORISE
Subtask 3.3 – Methodology Developments for Modeling Geomechanical Stability of Hydrate-Bearing Sediments under Hydrate Dissociation Condition	Yongkoo Seol	NETL-ORD
	Jeong-Hoon Choi	ORISE
Task 4.0 – Pore-Scale Visualization and Characterization of Hydrate-Bearing Sediments		
Subtask 4.1 – Effect of Continuous Brine Flow on Hydrate Formation and Dissociation Behaviors	Yongkoo Seol	NETL-ORD
	Sheng Dai Terrance Ryan Matthew Tacker	ORISE
Subtask 4.2 – Water and Gas Distributions after Hydrate Dissociation and Implications to Permeability	Yongkoo Seol	NETL-ORD
	Sheng Dai Terrance Ryan Matthew Tacker	ORISE
Subtask 4.3 – Links between Hydrate Morphologies and Geomechanical Properties	Yongkoo Seol	NETL-ORD
	Sheng Dai Terrance Ryan Matthew Tacker	ORISE
Subtask 4.4 – Microfluidic-Based Permeability of Hydrate-Bearing Sediments	Yongkoo Seol	NETL-ORD
	Sheng Dai Terrance Ryan Matthew Tacker	ORISE

Note: The Hydrates FY15 FWP was written at the originally requested $800K scope, funded by FY14 (~$469K) and FY15 (~$330K) funds. However, due to the unpredictable circumstances regarding site-support contracts for university faculties and students, all activities within the Statement of Project Objectives will not be initiated until qualified researchers or students are identified. The activities that will not be initiated until full staff supporting is identified are highlighted in gray.